العنوان:	Analyzing the Climate Change Induced Variations in Intensity - Duration - Frequency Curves in Tawi Atair, Oman
المؤلف الرئيسي:	بني عرابة، محمود محمد
مؤلفين آخرين:	Gunawardhana, Luminda(Advisor)
التاريخ الميلادي:	2017
موقع:	مسقط
الصفحات:	1 - 64
رقم MD:	961771
نوع المحتوى:	رسائل جامعية
اللغة:	English
الدرجة العلمية:	رسالة ماجستير
الجامعة:	جامعة السلطان قابوس
الكلية:	كلية الهندسة
الدولة:	عمان
قواعد المعلومات:	Dissertations
مواضيع:	تغير المناخ، منحنيات الكثافة، سلطنة عمان، تقنية البعثرة غير الخطية، مياة الامطار
رابط:	http://search.mandumah.com/Record/961771

ANALYZING THE CLIMATE CHANGE-INDUCED VARIATIONS IN INTENSITY-DURATION-FREQUENCY CURVES IN TAWI ATAIR, OMAN

Mahmoud Mohammed Bani Uraba

A thesis submitted in partial fulfilment of the
requirements for the degree
Masters of Science in
Civil Engineering

Department of Civil and Architectural Engineering
College of Engineering
Sultan Qaboos University
Sultanate of Oman

April 2017

Thesis of: Mahmood Bani Araba (I.D. #) 046873

Title of Thesis: Analyzing the climate change-induced variations in Intensity-Duration-Frequency curves in Tawi Atair, Oman

Thesis Committee:

1. Supervisor: Dr. Luminda Gunawardhana
   Title: Assistant Professor
   Department: Civil and Architectural Engineering
   Institution: Sultan Qaboos University
   Signature: Date: 4/5/2017

2. Member: Dr. Ghazi Al-Rawas
   Title: Assistant Professor
   Department: Civil and Architectural Engineering
   Institution: Sultan Qaboos University
   Signature: Date: 7/5/2017

3. Member: Dr. Mahad Baawain
   Title: Associate Professor
   Department: Civil and Architectural Engineering
   Institution: Sultan Qaboos University
   Signature: Date: 4/5/2017

Thesis Examination Committee:

1. Chair: Dr. Abdullah Al-Shabibi
   Title: Assistant Professor
   Department: Mechanical and Industrial Engineering
   Institution: Sultan Qaboos University
   Signature: Date: 9/5/2017

2. Supervisor: Dr. Luminda Gunawardhana
   Title: Assistant Professor
   Department: Civil and Architectural Engineering
   Institution: Sultan Qaboos University
   Signature: Date: 4/5/2017

3. Member: Dr. Muhammed Al-Mamun
   Title: Assistant Professor
   Department: Civil and Architectural Engineering
   Institution: Sultan Qaboos University
   Signature: Date: 4/5/2017

4. External Examiner: Dr. Malik Al-Wardy
   Title: Assistant Professor
   Department: Soils, Water and Agricultural Engineering
   Institution: Sultan Qaboos University
   Signature: Date: 4/5/2017

ACKNOWLEDGEMENT

First of all, I praise and thank almighty Allah for his blessings bestowed upon us. Then, I would like to express my deepest gratitude to my thesis supervisor Dr. Luminda Gunawardhana for his continuous support and guidance throughout the study period. His kindness and patience are unforgettable.

I would also like to express my thanks to the faculty of the Department of Civil and Architectural Engineering in the Sultan Qaboos University for their usual support and assistance. Especially the internal committee of my thesis, Dr. Ghazi Al-Rawas and Dr. Mahad Baawai, the external examiner Dr. Malik Al-Wardy, the chairman of examination committee Dr. Abdullah Al-Shabibi as well as Dr. Muhammed Al-Mamun.

Special thanks to the Ministry of Regional Municipalities and Water Resources & the Public Authority for Civil Aviation for providing the necessary data required to carry out the study. This is to specially thank Eng. Tariq Hilmy and Dr. Said Al-Sarmi for their kindness and support.

I am very much grateful to my company, Ooredoo Oman and my co-workers and colleagues at work for their understanding and motivations through the assigned period for completing my Master's Degree. This is to thank Fadi Hiyari for his support in implementing the K-NN method in excel worksheet.

Last but not least, I express my heartfelt appreciation and thankfulness to my parents for all the efforts they made to raise me and make me the person I am. A loving thanks to my wife for her patience and encouragement that helped me in completing my study seamlessly.

ABSTRACT

Climate change affects different areas of our lives. The rise in the mean sea level, increases in temperature and changes in intensity and frequency of extreme events attributed to climate change lead to many socio-economical complications. Water management systems depend on the hydrological inputs for the engineering design. The main input for such designs, the Intensity-Duration-Frequency (IDF) curves, which were thought to be stationary is actually altered significantly with the changes in the extreme rainfall events. This paper discusses the possible variations in the IDF curves due to the climate change in Tawi Atair, Dhofar. It begins with the development of historical IDF curves and then utilizing two General Circulation Models (GCM's) from the Couple Model Intercomparison Phase 5 (CMIP5) for the future projections of IDF curves during the years 2040-2059 and 2080-2099 by considering two emission scenarios, RCP4.5 and RCP8.5. A two-stage downscaling-disaggregation method was applied. Firstly, low spatial resolution GCM results were downscaled to the site-specific scale using weather generator (Lars-WG). Secondly, a non-parametric disaggregation technique, known as the K-Nearest Neighbor (KNN), was used to disaggregate GCM daily time series to the hourly and sub-hourly time scales.

The two GCM's were selected among 5 GCM's based on their performance to simulate the local precipitation in the Salalah region during 1950-2005. Accordingly, CNRM-CM5 and MRI-CGCM3 models were selected. The Lars-WG was calibrated with the observations of the study area for the years 1993-2009. The K-NN optimum disaggregation models for hourly and sub-hourly disaggregation were obtained based on the window size approach. The optimum window sizes for the hourly and sub-hourly disaggregation were found to be 28 days and 90 hours, respectively.

The results show that the rainfall intensities are increasing especially for the short duration storms. For example, rainfall intensity of 5-min and 1-hr storms with 25-yr return period have increased by 51% and 14% respectively. The level of uncertainty related to different factors such as the methods used, the GCM's and RCP's selected and the statistical fitting of the Annual Maximum Rainfalls (AMR's) to the probability distribution function were discussed and presented in different formats for broader understanding.

العنوان: تحليل التغيرات المتعلقة بتغير المناخ على منحنيات الكثافة-الفترة-والتردد في نيابة طوي أعتير، سلطنة عمان

محمود بني عرابة

الملخص

يؤثر التغير المناخي على نواح مختلفة من حياتنا. ارتفاع منسوب مياه البحر، وارتفاع درجات الحرارة وأنواء الطقس الشديدة بسبب تغير المناخ يؤدي إلى العديد من المشاكل المتعلقة بالمجتمعات والإقتصاد. أنظمة إدارة المياه تعتمد أساسا على البيانات المائية من أجل التصميم الهندسي. الركيزة الأساسية لهذه البيانات، ما يسمى بـ منحنيات الكثافة-الفترة-والتردد (IDF CURVES)، والتي كان يعتقد بأنها ثابتة لا تتغير، هي في الحقيقة تتأثر إلى حد كبير كلما زادت الأنواء المطرية الشديدة. يناقش هذا البحث التغيرات التي من الممكن أن تطرأ على منحنيات الكثافة-الفترة-والتردد نتيجة لتغير المناخ في **نيابة طوي أعتير، بمحافظة ظفار.** تبدأ العملية برسم منحنيات الكثافة-الفترة-والتردد للسنوات الماضية، ثم بعد ذلك وباستخدام نموذجين من النماذج المناخية العامة (GCM) المدرجة تحت ال (5 CMIP) من أجل التنبؤ المستقبلي لمنحنيات الكثافة-الفترة-والتردد خلال الفترات من 2040-2059م و 2080-2099م باعتبار سيناريوهين انبعاثيين، 4.5 RCP و 8.5 RCP.

الآلية التي تم اتباعها في هذا البحث هي آلية الإسقاط القياسي – والبعثرة البيانية والتي تجمع بين الإسقاط القياسي للنماذج المناخية العامة ذات الدقة المكانية الرديئة على مقياس المنطقة المحددة باستخدام مولد الطقس (Lars-WG)، وبين بعثرة بيانات النماذج المناخية العامة المعتمدة على التنبؤ اليومي إلى بيانات ساعاتية و تحت - ساعاتية باستخدام تقنية البعثرة الغير –معيارية، الـ " كي-إن إن" (K-NN).

النموذجان المناخيان تم اختيارهما من بين خمسة نماذج حسب أدائها في محاكاة بيانات الأمطار المسجلة في صلالة لأنها الأطول مدة (1950-2005م) من بين المحطات الأخرى في المنطقة. أفضل هذه النماذج كان نموذج CNRM-CM5 ونموذج MRI-CGCM3.

لقد تم معايرة مولد الطقس من خلال بيانات الأمطار المسجلة في طوي أعتير خلال السنوات (1993-2009م). بالمقابل، فإن نماذج البعثرة البيانية المثلى قد تم تطويرها باستخدام طريقة حجم النافذة الوقتية (window size approach). كانت حجم النوافذ الوقتية المثلى التي تم تحصيلها لنموذجي البعثرة البيانية الساعاتي والتحت ساعاتي، 28 يوما و 90 ساعة، على التوالي.

تشير النتائج إلى ارتفاع في معدلات كميات الأمطار لاسيما في العواصف القصيرة المدى، على سبيل المثال، فإن العواصف ذات الخمس دقائق والعواصف ذات الساعة زادت بنسبة 51 في المئة و 14 في المئة على التوالي. هامش الخطأ المتعلق بعوامل مختلفة، على سبيل المثال، الطرق المستخدمة، النماذج المناخية والسيناريوهات الإنبعاثية المستخدمة، بالإضافة إلى عملية المماثلة الإحصائية بين االكثافة السنوية القصوى للأمطار (AMR) وبين دالة توزيع الإحتمالات (PDF)، تم نقاشها وعرضها بأساليب مختلفة لتعميق الفهم.

TABLE OF CONTENTS

List of Tables

List of Figures

ACRONYMS & ABBREVIATIONS

°C	Degrees Celsius
AMR	Annual Maximum Rainfall
ANN	Artificial Neural Network
AR4	Assessment Report 4
AR5	Assessment Report 5
BLRP	Bartlett-Lewis Rectangular Pulses
CMIP3	Coupled Model Intercomparison Project Phase 3
CMIP5	Coupled Model Intercomparison Project Phase 5
ECP	Extended Concentration Pathways
ETCCDI	Expert Team on Climate Change Detection and Indices
GCM	General Circulation Model
GEV	Generalized Extreme Value
GHG	Greenhouse Gases
GLM	General Linear Model
GP	Genetic Programming
hr	Hour
IDF	Intensity-Duration-Frequency
IPCC	Intergovernmental Panel on Climate Change
K-NN	K-Nearest Neighbor
K-S test	Kolmogorov-Smirnov test
Lars-WG	Long Ashton Research Station- Weather Generator
min	Minute
MLE	Maximum Likelihood Estimate
MRMWR	Ministry of Regional Municipalities and Water Resources
PACA	Public Authority for Civil Aviation
PD	Peak-Decline
PDF	Probability Distribution Function
RCF	Relative Change Factor
RCP	Representative Concentration Pathway
RMSE	Root Mean Squared Error
SD	Standard Deviation
TN10p	Percentage of days when daily minimum temperature is less than 10^{th} percentile
TN90p	Percentage of days when daily minimum temperature is greater than 90^{th} percentile
Watt/m2	Watts per square meter
WMO	World Meteorological Organization
yr	Year

CHAPTER 1: INTRODUCTION

1.1 General Introduction

Extreme weather/rainfall events are showing increasing trends in the world. Scientists attribute the increase in the intensity of the rain and snowstorms to the climate change (i.e. Global Warming). Alexander et al. (2006) found that the precipitation indices show a tendency toward wetter conditions throughout the 20th century. The physical mechanism behind the link between global warming and stronger rainfall is explained by the Clausius-Clapeyron equation. As climate warms, saturation vapor pressure rises exponentially, and the water holding capacity of the atmosphere increases by approximately 7% per 1°C. As a result, the amount of moisture in the atmosphere increases. Trenberth et al. (2003) argued that, consequently, the rainfall intensity (heavy events above 85th percentile) should also increase at approximately the same rate or can even exceed 7% per 1 °C. The Fifth Assessment Report (AR5) of the United Nations Intergovernmental Panel on Climate Change (IPCC) concluded that the rise in the mean global surface air temperature by the end of the 21st century, relative to the pre-industrial period, is likely to be between 1.5°C and 4.5°C (Symon 2013).

In Oman, almost every year, a cyclone or more of different categories hit the country across the northern part. Before Cyclone Gonu (2007), insufficient attention has been paid towards cyclonic events as almost no Gonu-like event was experienced, at least not with that much of intensity in a short period of time. This has triggered the efforts of researches to study the extreme weather events and take the necessary measurements to divert the attendant consequences to the benefit of the people and country.

In Salalah (Capital of Dhofar governorate), Al-Habsi et al. (2014) observed that the mean annual temperature during 1980-2008 warms at a rate of 0.12°C/10-years. If such rate continues steadily, then the rainfall intensity is expected to intensify towards the end of the 21st century.

Under changing climate conditions in Oman, exclusive use of climatic normals derived from historical data may no longer be appropriate and could render infrastructure vulnerable by leading to designs with insufficient capacity, or by taking policy measures that become difficult to practice over time. The use of climate data in the planning and design of infrastructure may avoid, or at the very least reduce, future economic, social and environmental damages.

In light of the above, one of the important topics that is being studied in many countries around the world is the intensity-duration-frequency curves (IDF curves). These curves are basically combining the intensity duration and frequency (return period) parameters of a storm in a graphical relationship through a statistical formula. Many places around the world depend on the IDF curves for the design of different hydro-systems such as storm water channels, drainage systems, culverts, dams, etc. (Alam and Elshorbagy, 2015). The classical method for constructing the IDF curves begin with the assumption that the rainfall extremes recurrence intervals are stationary. However, under the changing climate conditions, this assumption would make the historical IDF curves unacceptable for future conditions. This study is an attempt to review the historical IDF curves in *Tawi Atair* (having the longest 5-min rainfall records in the region) and produce future IDF curves through the General Circulation Models under the emission scenarios adopted by the fifth assessment report (AR5) of the Intergovernmental Panel on Climate Change (IPCC).

1.2 Objectives

The objective of this study is to project variations in extreme rainfall in *Tawi Atair* in future considering General Circulation Models (GCM's) under Representative Concentration Pathways (RCP's) scenarios and incorporate them to develop a new set of IDF curves.

Another target is to evaluate several GCM's and identify the ones that best simulate the rainfall patterns in the region which can assist researchers to directly consider them for climate change studies. In addition, the optimum window size for disaggregation which represents the most appropriate memory length of the hydrological system in the region is also targeted.

Furthermore, it is aimed through this research to obtain downscaled disaggregated future data that can be used for similar studies and establish a methodology that can be adopted by researchers in Oman to apply in other regions.

1.3 Research Procedure

The research procedure adopted in this report includes several stages starting from planning, method statement, rainfall data collection, data preparation and quality verification, models and tools design and calibration, implementation and analysis, results collection and report preparations.

The following points summarize the adopted steps:

- Research Planning: in this stage, the research overall plan that covers the subject, main objective, location of interest, source of data provision, the research milestones and expected results were identified.
- Method statement: the procedure and tools to be used were identified. Lars-WG was selected for downscaling process, K-NN method was selected for disaggregation process. R-extreme toolkit was selected for the GEV distribution fitting process.
- Rainfall data collection: the data were collected from the Ministry of Municipalities and Water Resources for all stations in Dhofar region. Out of more than 10 stations, the station of Tawi Atair was selected as it has the longest records of sub-hourly rainfall records.
- Data preparation and quality verification: the rainfall data were verified to check errors and outliers. Also, the data were re-arranged in a 5-min step intervals which is necessary for a consistent analysis.
- Models and tools design and calibration: the selected techniques and softwares were prepared for the implementation. The Lars-WG was calibrated with site-specific observations of Tawi Atair. The K-NN model for hourly and sub-hourly disaggregation were prepared using macro-enabled excel sheet for automated data processing. The R-

extreme toolkit coding and procedure were prepared and verified by another commercial software 'easy fit' (trial version).

- Implementation and analysis: the future and historical GCM data were downloaded, downscaled by Lars-WG, disaggregated by K-NN and processed by R-extremes/easy fit and IDF results were generated.

1.4 Organization of the Thesis

The thesis starts with a general introduction, main objectives and research procedure in Chapter 1. Literature review which covers previous studies, definitions and different aspects of the climate change techniques are discussed in Chapter 2. Chapter 3 describes the study area in terms of geographical location and climate with brief trend analysis of rainfall in the area. Detailed description of the methodology and processes followed are shown in Chapter 4. Chapter 5 presents the results and discussions that covers the methods results and variation analysis. Finally, Conclusions and recommendations are presented in the last chapter of the thesis, Chapter 6.

CHAPTER 2: LITERATURE REVIEW

2.1 General Background

In the Arabian Peninsula, very few studies have focused on the climate extremes analysis (AlSarmi and Washington, 2013). AlSarmi and Washington (2013) analyzed the observed temperature and precipitation records from 23 stations covering the six Arabian Gulf countries using climate extremes indices developed by the Expert Team on Climate Change Detection and Indices (ETCCDI) and R-based software (RclimDex) which is developed and maintained by Xuebin Zhang and Feng Yang at the Climate Research Branch of Meteorological Service of Canada. The results showed a general decreasing trend of cold temperature extremes and increasing trends of the warm temperature extremes during the periods of analysis. Also, high increase in very warm nights (TN90p) during 1986–2008 was observed with no significant trends in the indices of the precipitation extremes. However, it was observed that the annual count of days when precipitation exceeds 10mm have significant decreased.

Another study by Al-Habsi et al. (2014) employed the same indices for precipitation and temperature at Salalah over the periods 1943-2011 and 1991-2011, respectively. The analysis of the temperature records agrees with the results obtained by AlSarmi and Washington (2013). The annual number of cold nights (TN10p) has decreased by 8 days and on the other hand the warm nights has increased by 10 days. It was also concluded that the contribution from the very wet days R95P has increased, whereas the total precipitation averaged over the study period has shown negative trend with a rate of -2mm/10yr.

It should be noted that the extreme indices are more suitable in the assessment of moderate extremes that typically occur a few times every year rather than high-impact, multi-decade weather events which are important in the design of hydro-systems. Events that lie far in the tails of the probability distributions require fitting a statistical model to the annual extremes in a time series of data (WMO, 2009). This is commonly applied based on the extreme value theory employing the Generalized Extreme Value (GEV) distribution. Together with the help of General Circulation

Models (GCM's), researchers could project future climate change-induced variations on weather variables.

The current storm water collection systems are designed using historical IDF curves in many places but they are subject to change due to climate change impacts (Watt and Marsalek, 2013). According to the available literature, no previous study has covered the effects of climate change on IDF curves in Oman. This would obviously increase the vulnerability of the respective infrastructures leading to catastrophes in future under changing climate conditions. Thus, it would be very important to first construct the IDF curves for the baseline period and investigate the future projections under the climate change scenarios.

2.2 General Circulation Models

Investigating the climate change effects on future rainfall extremes through the GCMs is a common practice worldwide. The GCM's are used to assess the global climate change by representing the different chemical and physical atmospheric, oceanic and land processes with numerical modelling.

Gunawardhana et al. (2015) investigated how the magnitude and occurrence of extreme precipitation events are affected by climate change and predicted the subsequent impacts on the *wadi* flow regime in the Al-Khod catchment area, Muscat, Oman. Six GCMs from the Coupled Model Intercomparison Project Phase 5 (CMIP5) under different Representative Concentration Pathways (RCP's) were used to analyze precipitation extremes and their future potential changes. The results indicated that extreme precipitation events consistently increase by the middle of the twenty-first century for all return periods (49–52 %) and (81–101 %) by the end of the twenty-first century.

The GCMs simulations of climate variables in the previous experiments were based on six emission scenarios under four families (A1, A2, B1 and B2) known as 'Special Report Emission Scenarios, SRES' from the Coupled Model Intercomparison Project Phase 3 (CMIP3). These scenarios were replaced with the emergence of the Fifth Assessment Report (AR5) of IPCC based

on Phase 5 (CMIP5), where a new set of GCMs simulations was presented to the research community under new emission scenarios called 'Representative Concentration Pathways (RCP's)'.

There are four RCPs considered in the IPCC AR5 defined by their total radiative forcings, which is a measure of the cumulative effect of human emissions of GHGs from all sources and is expressed in watts per square meter. Therefore, the RCP2.6, RCP4.5, RCP6.0, and RCP8.5 scenarios represent pathways that result in radiative forcings of 2.6, 4.5, 6.0, and 8.5 W/m^2, respectively in 2100 (Moss et al., 2010). Table 1 shows the new emission scenarios (RCPs) characteristics, emissions weightage and their temperature anomaly equivalent from the SRES.

Table 1 RCPs emissions units and characteristics with equivalent SRES scenarios, Moss et al. (2010).

Name	Radiative Forcing	CO2 equivalent (p.p.m.)	Temp anomaly °C	Pathway	SRES temp anomaly equiv
RCP8.5	8.5 Wm^{-2} in 2100	1370	4.9	Rising	SRES A1F1
RCP6	6.0 Wm^{-2} in 2100	850	3	Stabilization without overshoot	SRES B2
RCP4.5	4.5 Wm^{-2} in 2100	650	2.4	Stabilization without overshoot	SRES B1
RCP2.6 (RCP3PD)	3 Wm^{-2} before 2100, declining to 2.6 Wm^{-2} by 2100	490	1.5	Peak and decline	None

Each individual RCP is described in details in the papers by Riahi et al. (2011), Masui et al. (2011), Thomson et al. (2011) and Van Vuuren et al. (2011) for RCP8.5, RCP6, RCP4.5 and RCP2.6 respectively. These papers provide brief explanation on the modeling systems that have created each RCP, the main socio-economic assumptions, the underlying trends in energy use and details on emissions and land use. In addition, the papers discuss alternative scenarios that represent forcing levels similar to the four main RCPs.

Meinshausen et al. (2011) have expanded the RCPs projection beyond 2100 to reach the year 2300. The RCPs are divided into three categories. The RCP 2.6 (or RCP3PD, peak-decline) which represents a strong mitigation plan having the lowest radiative forcing found in literature. Secondly, two intermediate or medium stabilization scenarios (RCP4.5 & RCP 6.0) which cover a wide range of scenarios in the literature. The third one has the highest level of radiative forcing,

RCP 8.5 with an increasing trend until 2200. Table 2 shows the RCPs with their extensions, ECPs, and the extension rule governing the behavior along the line to 2300. Figure 1 illustrates the trajectories of each scenario from 1800-2300.

Table 2: The RCPs and their simple extension rules beyond 2100 assumed for all GHGs, Meinshausen et al. (2011).

RCP scenario 2005-2100	Extension 2100 to 2300	Extension rule
RCP2.6/RCP3-PD	ECP3-PD	Constant emissions after 2100.
RCP4.5 RCP6	ECP4.5 ECP6	Smooth transition towards concentration stabilization level after 2150 achieved by linear adjustment of emission between 2100 and 2150.
RCP8.5	ECP8.5	Constant emissions after 2100, folllowed by a smooth transition to stabilized concentrations after 2250 achieved by linear adjustment of emissions after 2150.
RCP6	Supplementary Extension SCP6to4.5	Adjustment of emissions after 2100 to reach RCP4.5 concentration levels in 2250 and thereafter.

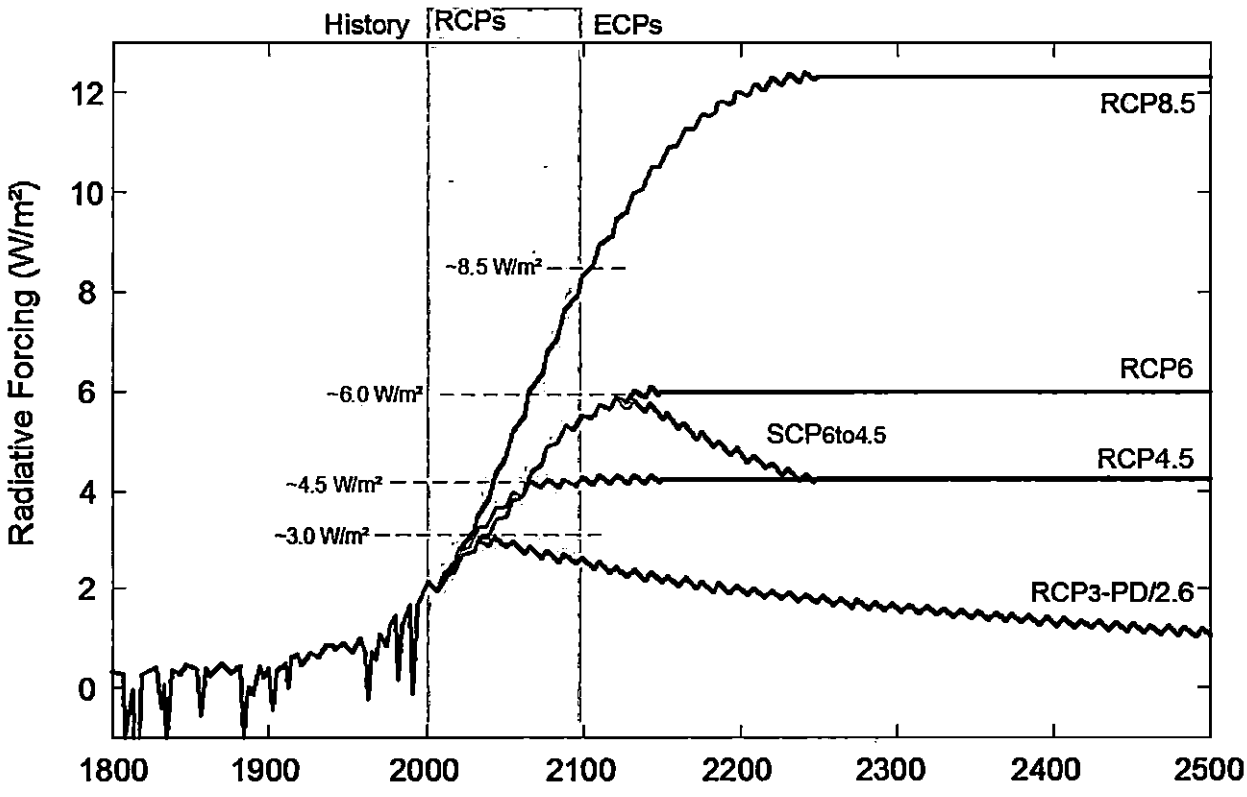

Figure 1 Total radiative forcing for RCPs and their extensions ECPs (1800-2300), Meinshausen et al. (2011)

However, the GCM's used for future projections generate results in coarse spatial resolution which doesn't allow for reliable impact studies as the information provided by these models come at a horizontal scale of 100-300 km which is too coarse to be considered in the climate change studies of extreme climate and weather forecast. Therefore, researchers apply downscaling techniques to overcome this issue.

2.3 Downscaling Methods

The main downscaling methods are the dynamical and the statistical downscaling. The dynamical downscaling uses a Regional Climate Model (a local high resolution numerical model) driven by the boundary conditions of a global climate model to derive smaller scale climate variables. This method is quite extensive in terms of computational efforts and cost. It also requires vast knowledge in climate modeling. The statistical downscaling involves forming a statistical relationship between the local scale variables to those in the GCM's output to generate synthetic variables that carry the local scale statistical characteristics. This method requires less computational effort and therefore can be considered in the future projections using ensembles of GCM's which is recommended in the climate change impact studies. The following sub-section discussed the types of statistical downscaling in more details.

2.3.1 Statistical Downscaling

There are three types of statistical downscaling; regression-based methods, weather typing approaches, and stochastic weather generators (Wilby and Wigley, 1997).

Regression-based methods:

This method involves developing a relationships between the global scale variables (e.g. rainfall) and the local scale variables. Different types of regression-based downscaling techniques are available in literature, such as multiple linear regression, SDSM (Wilby et al., 2002), canonical correlation analysis (Busuioc et al., 2008), and genetic programming-based method (Hassanzadeh et al., 2014).

Mishra et al. (2014) used the multiple linear regression-based statistical downscaling, to establish relationship between the GCM-scale and the local scale. They have calibrated and validated the model using screened large-scale predictors of (National Centre for Environmental Prediction (NCEP) and analyzed future rainfall projections based the British GCM (HadCM3) under A2 scenario. The calibration-validation results confirm the statistical downscaling model acceptability slightly at a lower degree. Hassanzadeh et al., (2014) used the genetic programming as statistical downscaling method. The algorithm used in this method maps the relationship between rainfall quantiles at both global and local scale without having to generate a continuous rainfall time series.

Weather typing/classification:

In this method, the local variable is predicted based on large-scale atmospheric "states." The states can be identifiable synoptic weather patterns or hidden, complex systems. The future atmospheric state, simulated by a GCM, is matched with its most similar historical atmospheric state. The selected historic atmospheric state then corresponds to a value or a class of values of the local variable, which are then replicated under the future atmospheric state. This method is well suited for downscaling non-normal distributions, such as daily rainfall. However, a large number of observational daily records (e.g., 30 years of daily records for the area of interest) is required to evaluate natural weather variability. Furthermore, the method requires extensive computations when compared with the regression-based ones, due to the amount of data analyzed and generated. Willems and Vrac (2011) made a comparison between the weather typing downscaling method and a quantile-perturbation based method (regression-based) for investigating of the changes in the IDF curves in Belgium. The two methods produced the short duration precipitation extremes similarly. The weather typing method in this case used temperature as a large-scale predictor in addition to the atmospheric circulation.

Stochastic weather generation:

Stochastic weather generators produce synthetic time series of weather data of unlimited length for a location based on the statistical characteristics of observed weather at that location. Stochastic weather data are generated by models that are developed in two steps (Hutchinson, 1987). The first

step is to model daily precipitation and the second step is to model the remaining variables of interest, such as daily maximum and minimum temperature, humidity, solar radiation... etc.

Probably the best known approach for developing weather generators was reviewed by Richardson (1981), and weather generators that followed adopting this approach are often referred to as the "Richardson-type". The main limitation of the Richardson-type WG is its failure to sufficiently describe the length of dry and wet series (the extreme weather like droughts and floods).

An alternative approach, follows the "serial approach", has been developed by (Racsko et al., 1991), which models the sequence of dry and wet series of days first and then models other weather variables like rainfall amount and temperature as a result of the wet or dry series modelling. An example of series approach weather generators is Lars-WG (Long Ashton Research Station-Weather Generator). Lars-WG is a popular stochastic weather generator tool for climate change impact studies and has been successfully applied around the world with different climate types (Lu, 2015). It is capable of simulating synthetic precipitation time series with statistical characteristics corresponding to the observed statistics at a site (Semenov and Barrow, 2002). The Lars-WG can serve as a computationally inexpensive tool to produce multiple-year climate change scenarios at the daily time scale which incorporate changes in both mean climate and in climate variability (Semenov and Barrow, 1997).

The weather generation process in LARS-WG is based on semi-empirical distribution (SED), which is defined as the cumulative probability distribution function describing the probability that a random variable with a given probability distribution takes on a value on the high or low extremes. Rest of the values are distributed evenly on the probability scale. The semi-empirical distribution is represented by a histogram with 23 semi-closed intervals indicating the distribution of events in the observed data. SED provides a flexible distribution with a possibility to approximate a wide range of shapes through adjustment of the intervals (Semenov and Barrow, 2002; Semenov and Stratonovitch, 2010).

Several studies have investigated the performance of LARS-WG compared to other statistical downscaling techniques and have confirmed that LARS-WG can be adopted with confidence as a

reliable downscaling technique in the climate change studies. LARS-WG was compared with another weather generator WGEN (Richardson, 1981), which uses the Markov procedure, at a number of sites with different climates and has been shown to perform very well compared to WGEN in all the sites considered (Semenov et al, 1998). Hashmi et al. (2011) compared the Lars-WG with a multiple regression-based model (SDSM) (Wilby et al., 2002). The results showed that both methods are acceptable with reasonable confidence as downscaling tools in impact assessment studies. Hashmi et al. (2009) analyzed the performance of LARS-WG for the Auckland (New Zealand) and concluded that it simulated the present climate and the future projections efficiently by using GCM outputs.

In this study, the Lars-WG version 5.5 was adopted for the downscaling process to downscale the GCM's coarse-scale output to a local-scale resolution for the base period as well as the future projections.

2.4 Rainfall Temporal Disaggregation

One common issue climate impact studies face is the lack of finer temporal resolution records which is very essential in the analysis and design of extreme weather events. To overcome this issue, the available coarse resolution records can be temporally disaggregated into finer time series via different techniques. There are number of disaggregation techniques available in the literature such as 'Bartlett-Lewis rectangular pulse model' (Rodriguez-Iturbe et al., 1987), 'multivariate rainfall disaggregation model' (Koutsoyiannis et al., 2003), 'Generalized linear model (GLM)' (Chandler and Wheater, 2002), 'Artificial Neural Networks' (Burian et al., 2000), and 'K-nearest neighbor (K-NN) technique' (Lall and Sharma, 1996).

Abdellatif et al. (2013) used Bartlett-Lewis Rectangular Pulses (BLRP) model coupled with a proportional adjusting procedure to disaggregate daily rainfall to hourly rainfall in three stations in England. Hanish (2016) discussed the applicability of the MuDRain (multivariate rainfall disaggregation) model for disaggregating daily rainfall to hourly rainfall for 7 gauges in Peninsular Malaysia. Wheater et al. (2005) used GLM to simulate daily precipitation coupled with poisson cluster process as a temporal disaggregation method to generate precipitation at finer resolutions.

Burian et al. (2000) evaluated two different ANN rainfall disaggregation models and compared their performance against two other rainfall disaggregation techniques: linear disaggregation method and continuous deterministic rainfall disaggregation model proposed by Ormsbee (1989). Results indicated that the ANN rainfall disaggregation models were comparable with the other disaggregation methods and performed better in predicting the maximum 15-min rainfall depth and the time this depth occurred.

In this study K-nearest neighbor (K-NN) - based time resampling approach, Lall and Sharma, (1996), was used for the temporal disaggregation of daily to hourly and hourly to sub-hourly. The K-NN technique is a nearest neighbor search method, also known as similarity or proximity search. The aim of this method is to identify the most similar or closest points to the point of interest among a pool of neighbors (data). The criteria for similarity or closeness is governed by Euclidean or Mahalanobis distance. This process can be defined as follows: if a domain (D) contains a set amount of points (P) and a point of interest (k) $\in$ D, K-NN looks for the nearest points (measured by the specified distance) to k in D (Liu, 2006). In this study, the pool of neighbors is represented by the historical rainfall records from which the closest point is to be found to simulate/disaggregate a point of interest in the future projections. Young (1994) employed a K-NN model for simulation of weather data that preserves the correlation between the temperature and the precipitation, and the wet or dry spell statistics. Sharif and Burn (2007) improved the K-NN weather generating model for resampling with perturbation of the historical data to produce new values while previous studies merely reshuffle the historical data to generate new weather sequences. Nowak et al. (2010) used K-NN to simulate daily stream flow at multisite from annual flow in the Southern Colorado. The results have captured the observed statistics quite well.

CHAPTER 3: STUDY AREA

3.1 Location

Oman is located in the southeastern part of the Arabian Peninsula. The area of the country is approximately 309 500 km^2. It has borders with United Arab Emirates (Northwest), Saudi Arabia (West), and Yemen (Southwest). Oman has a coastline of 2092 km extends from the Strait of Hormuz in the north to the borders of Yemen in the southwest. The land area comprises different geographical land which can be divided into three main geomorphic compartments (Kwarteng, 2009): Mountain chains (Al Hajar Mountains) with Altitudes more than 3000m (AMSL) extending from Musandam in the north towards the eastern part at Ras Al Hadd. Another Mountainous area located in the South (Dhofar Mountains) with altitudes that can reach upto 1800 m high (Al-Rawas and Valeo, 2010) overlooking the Indian Ocean. Both occupying 15% of the country.

The interior region is mainly desert land which occupies 82% of the country. The third compartment is the Coastal Plains (Al Batinah and Salalah Plains) which occupy 3% and are considered to be the main agricultural areas in the country. Tawi Atair is a small town under the Governorate of Dhofar located at the south of Oman (Figure 2). The study area, Tawi Atair is located in Dhofar Mountains 17.11° and longitude 54.52°, 20 km to the east of the capital of the Dhofar region, Salalah. It has an average elevation of 610m.

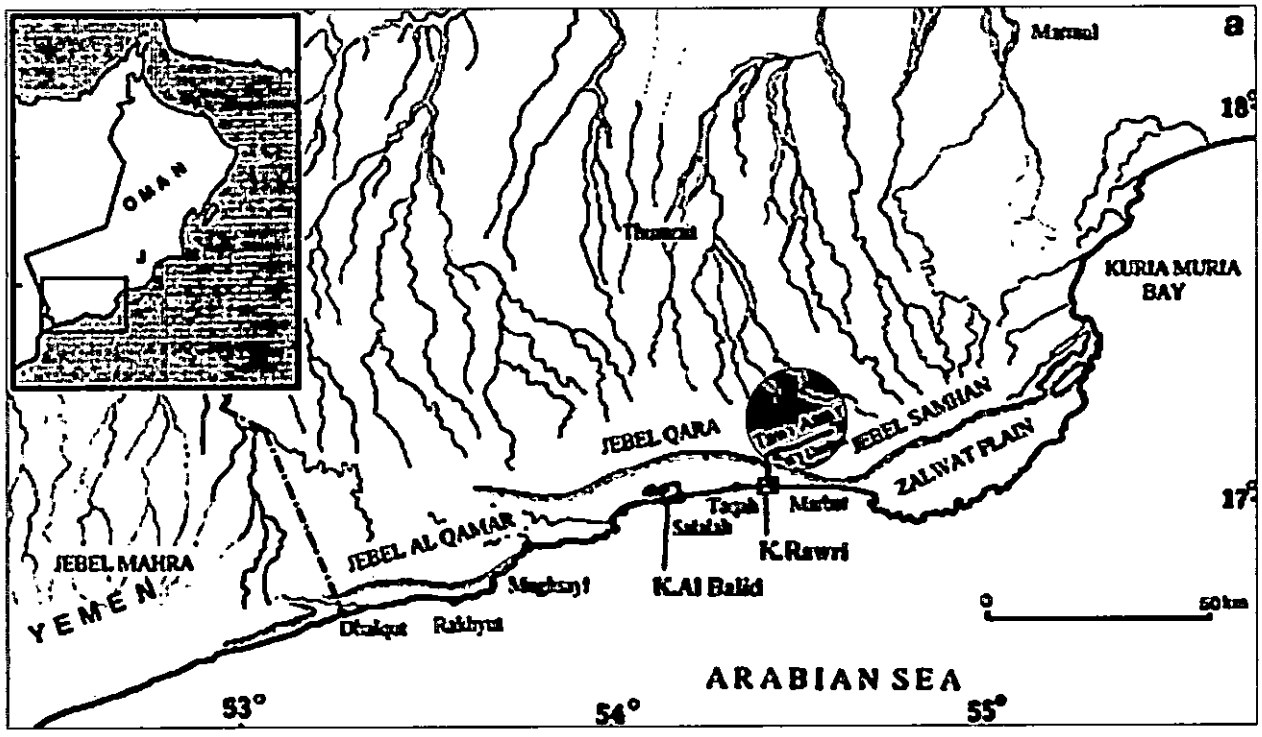

Figure 2 Study area in Oman

3.2 Climate

The climate in Oman varies from semi-arid to arid. In Northern Oman, the temperature from May to September ranges between 32 to 48 °C, and 26 to 36°C from October to April. Coastal regions are hot and humid in summer. In the interior region, maximum temperatures in summer can exceed 50 °C. Temperatures in winter are moderate ranging between 15 and 23 °C (Kwarteng, 2009).

The Dhofar region has fairly temperature around the year ranging between 30-35 °C. Four different rainfall mechanisms can be observed in Oman owns to the different physiographical regions discussed earlier (Kwarteng, 2009): *Convective rainstorms* mostly during the summer but can develop anytime of the year. *Cold frontal troughs* originating from the Mediterranean Sea most commonly from November to April. *Tropical cyclones* originating from the Arabian Sea during May-June and October-November cyclone seasons. *Monsoon currents* season in Dhofar Mountains and Salalah Plain in July and August accounting for 73 and 55% of the yearly rainfall respectively (Kwarteng, 2009). The rainfall in this season is characterized by light rainfall mainly drizzle, mist and fog. Gunawardhana et al. (2017) investigated the effect of climate change on the

number of wet days in Dhofar region in general and concluded that the NWD could decrease by 7.3 days and 3.3 days on average in the 2040-2059 and 2080-2099 periods, respectively. As such, the total annual rainfall is expected to decrease accordingly with major effect on the monsoon season.

Figure 3 shows the monthly total rainfall average over the period 1992-2015 in Tawi Atair. The effect of the monsoon season can be clearly seen for the months July and August. The total annual rainfall (*R_tot)* in this period is around 260 mm with an average number of wet days (days with rainfall more than 1mm) of 40 days/yr.

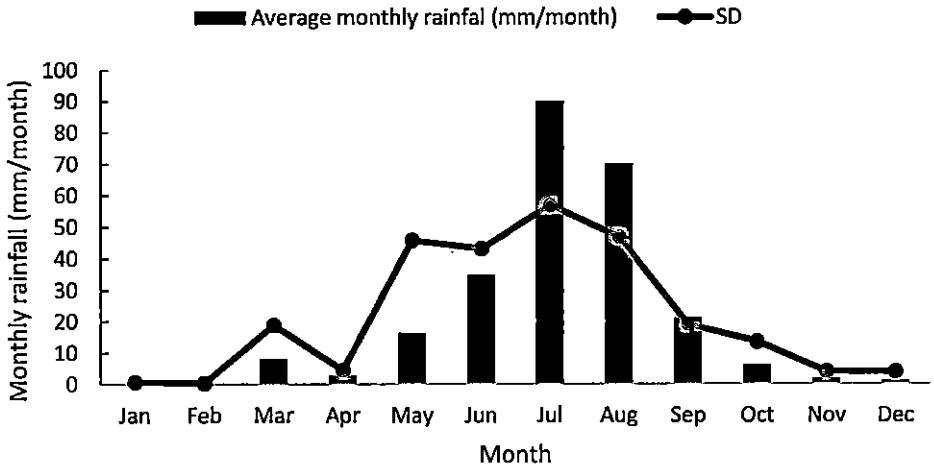

Figure 3 Monthly total rainfall average over the period 1992-2015 in Tawi Atair

Although the available rainfall dataset of the study covers the period (1992-2015) with missing records in the year 2010 as well as discontinuity for two years 2012 and 2013, the following figures are just an attempt to check the trends of the total annual rainfall (Figure 4) and the contribution from the very wet days (95^{th} percentile) to the total annual (Figure 5) both covering the continuous period of 1992-2009.

The negative linear trend of the total annual rainfall (see Figure 4) indicates a decreasing trend in the total annual rainfall and therefore can support the findings related to the effect of changing climate on the arid regions that such regions are expected to get dryer. On the other hand, major portion of the total annual rainfall are expected to be dominated by extreme rainfall events. Figure

5 shows the ratio of the 95th percentile to the total annual rainfall which can support the last claim as the trend line indicates an increase in the ratio. However, in order to draw solid conclusions in the trend analysis of weather variables, longer periods of records are required to accommodate the effect of natural fluctuations on the final trend line result.

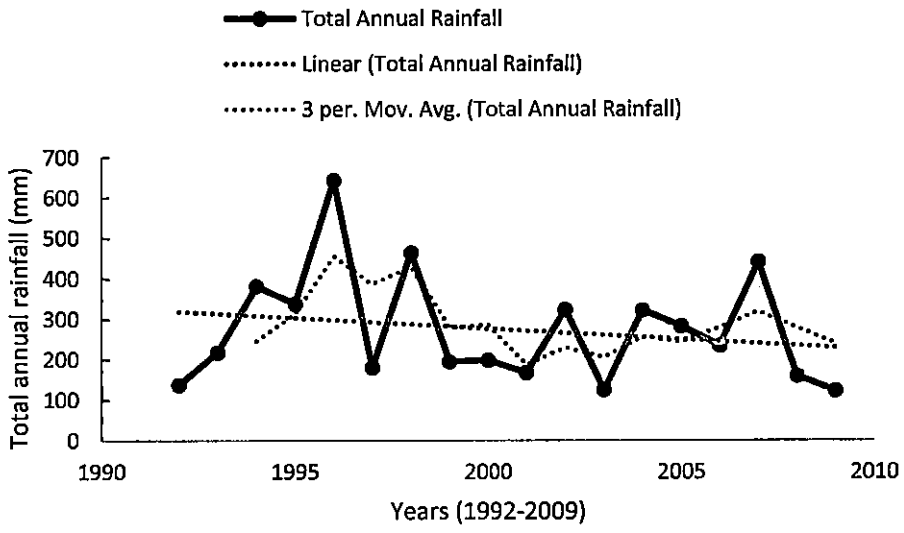

Figure 4 Total annual rainfall for the period 1992-2009

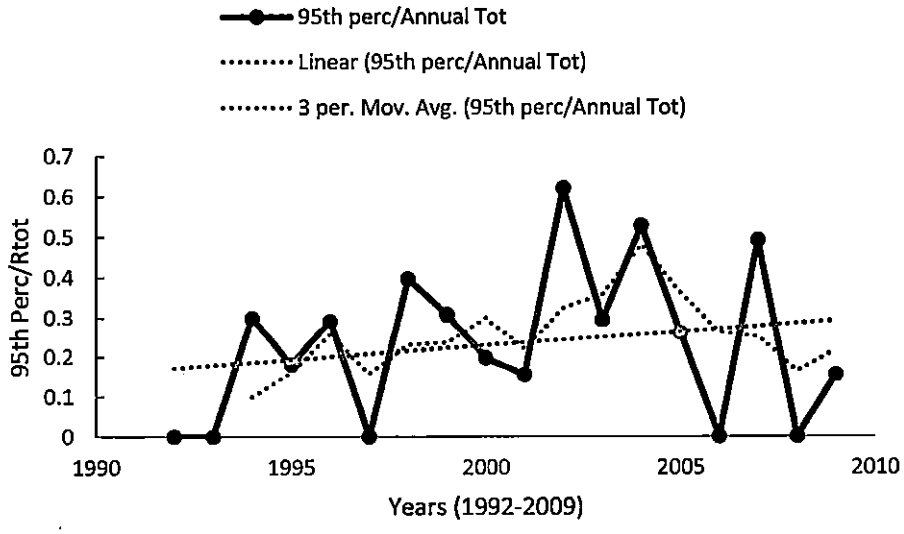

Figure 5 Contribution from very wet days (95th percentile) for 1992-2009

CHAPTER 4: METHEDOLOGY

4.1 Data and Method Summary

The rainfall data used in this study was obtained from a station at *Tawi Atair* which belongs to the Ministry of Regional Municipalities and Water Resources. The station is located at latitude 17.11° and longitude 54.52°.The data period extends from 1992 until end of 2015 with missing records from 2010 and a two-year discontinuity in the years 2012 and 2013. The complete data therefore comprises 22 years of daily record and 16 years of 5-min rainfall time series (1998-2015). This period was considered as the baseline period for the development and analysis of IDF curves. Another station in *Salalah* located at 17.02° and longitude 54.05 will be used for the selection of the GCMs purpose as it has the longest daily records. Table 3 shows the data sources and station locations.

Table 3 Rainfall data sources and duration

Rain Gauge Station	Source	Duration	Coordinates
Tawi Atair	Ministry of Regional Municipalities and Water Resources (MRMWR)	1992-2015	N 17.11° E 54.52 °
Salalah (Airport)	Public Authority for Civil Aviation (PACA)	1950-2005	N 17.02° E 54.05 °

The historical IDF curves were first constructed for the baseline period by fitting the GEV distribution on the annual maximum rainfall for eight durations from 5-min up to 24 hours and 5 return periods from 2-yr to 100-yr. Then, GCM data for five GCM's from the CMIP5 (Table 4) were downloaded for the baseline period and downscaled using stochastic weather generator (Lars-WG) to assess their performance in matching the local scale observations. The best two GCM's were selected to generate the future projections of daily rainfall for two time slices (2040-2059) and (2080-2099). After, that, a two-stage modeling (Alam and Elshorbagy, 2015) or a Combined Statistical Disaggregation Downscaling (CSDD) (Lu, 2015) method was followed in which the stochastic weather generator (LARS-WG) was used to downscale the selected GCM's future

projections to local scale and a K-nearest neighbor (K-NN) technique was used to disaggregate the downscaled daily rainfall to hourly and sub-hourly time series. A number of k-nearest neighbors were examined for Tawi Atair for both hourly and sub-hourly disaggregation models. Two optimal k-nearest neighbors were identified for the two disaggregation models. The weather generator, and the developed disaggregation models, were applied to the future projections through the application of the best two GCMs under two RCP's. Finally, The IDF curves were developed using the generalized extreme value (GEV) distribution to represent the annual maximum storm intensity. Figure 6 illustrates the method followed in a flow chart format.

Table 4: CMIP5 model names and scenarios used in this study.

CMIP5 model name	Modelling group	Grid resolution Lat × Lon
MIROC5	Center for Climate System Research (University of Tokyo), National Institute for Environmental Studies and Frontier	128 × 256
HadGEM2-ES	Hadley Centre for Climate Prediction and Research, UK	145 × 192
INM-CM4	Institute for Numerical Mathematics, Russia	120 × 180
CNRM-CM5	Meteo-France/Centre National de Recherches Meteorologiques, France	128 × 256
MRI-CGCM3	Meteorological Research Institute, Japan	160 × 320

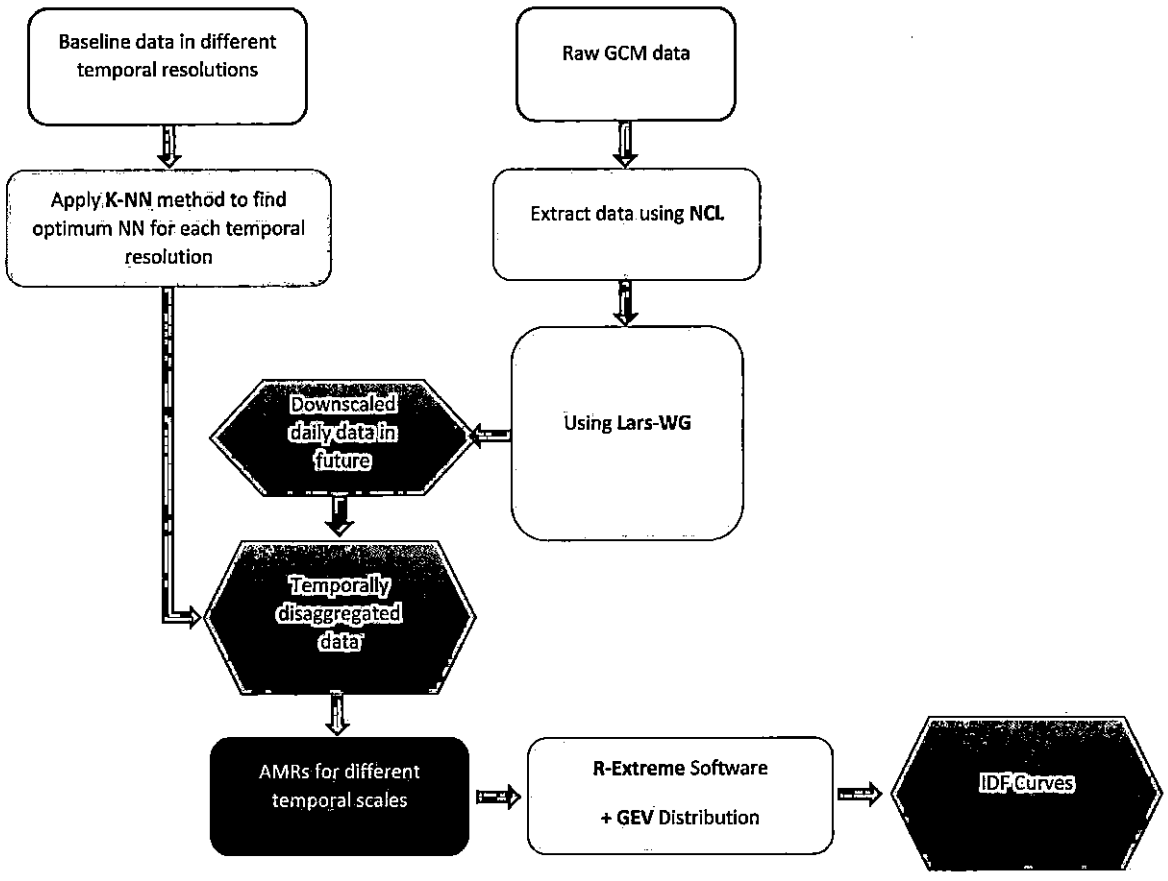

Figure 6 Flow Chart illustrating the steps followed in the study

4.2 General Circulation Models and Downscaling Process

Among the five GCM's (Table 4) downloaded from the portal, two GCM's were selected to produce the future projections for Tawi Atair. The criteria for the selection was based on the performance of each individual GCM to simulate the historical observations in terms of annual precipitation total, number of wet days, 95th percentile and daily maximum precipitation. The best two GCM's among the five (MRI-CGCM3 and CNRM-CM5) were used and their daily precipitation outputs were obtained from CMIP5 data portal for the baseline period (1998–2015) and two projection periods (2040-2059 & 2080–2099) based on two emission scenarios RCP 4.5 and RCP8.5. The raw GCM data for the local grid was extracted using NCL script.

The downscaling process was accomplished by using Lars-WG v5.5 (Long Ashton Research Station-Weather Generator). The Lars-WG version 5.5 was used to downscale the GCM's coarse-scale output to a local-scale resolution for the base period as well as the future projections. However, the latest version incorporates 15 GCM's based on the previous emission scenarios. Therefore, the new GCM's were downloaded from the CMIP5 portal and incorporated in the weather generator prior to downscaling process.

The downscaling process is illustrated in the flow chart as shown in Figure 7. First, the GCM data was extracted for the baseline and future periods. The data was analyzed by Lars-WG 5.5 in order to obtain the relative change factors for each month for wet and dry spell lengths as well as the mean rainfall. Scenario file was then created containing the monthly average of the relative change factors (RCFs) as rations of the future to the baseline period GCM records. The RCF's as well as the local observations in the baseline period were incorporated in Lars-WG 5.5 to run the downscaling process which uses the RCF's to perturb the parameters of the probability distribution of the observed records and generate future daily synthetic records having the local rainfall characteristics.

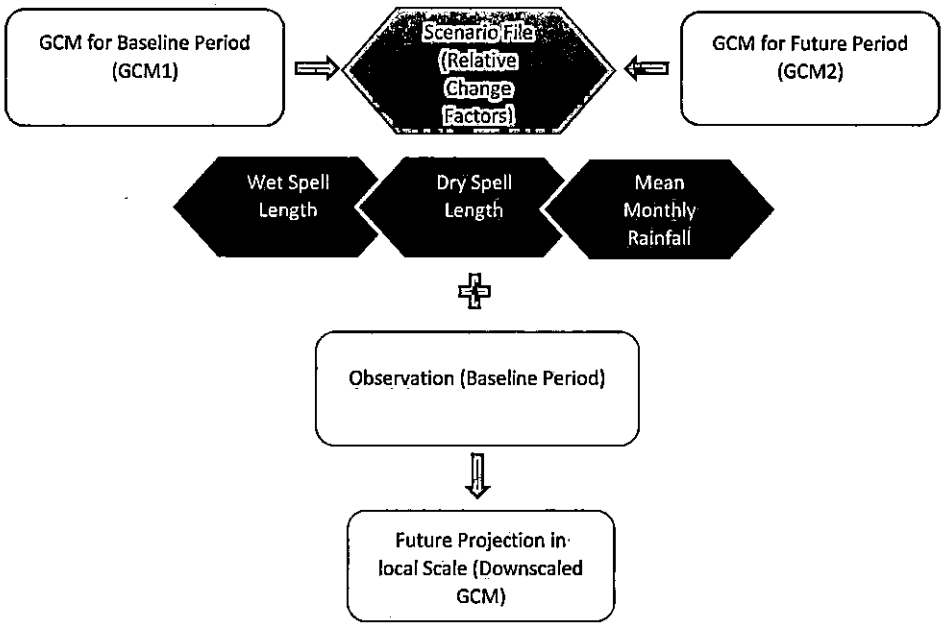

Figure 7 Flow Chart for Downscaling Process

4.3 K-Nearest Neighbor Disaggregation

K-NN disaggregation is a non-parametric technique used to disaggregate the daily weather variables into hourly and sub-hourly time series. The method is discussed in details in the following sub-section.

4.3.1 K-NN Method Procedure

The implementation procedures will follow Lu et al. (2015) which are explained through the following steps:

Step 1: Let $\boldsymbol{H}$ be the matrix containing observed hourly data, and $\boldsymbol{D}$ be the corresponding observed daily data:

$$H = \begin{bmatrix} h_{1,1} & \cdots & h_{1,j} & \cdots & h_{1,24} \\ h_{i,1} & \cdots & h_{i,j} & \cdots & h_{i,24} \\ h_{I,1} & \cdots & h_{I,j} & \cdots & h_{I,24} \end{bmatrix} \qquad D = \begin{bmatrix} d_1 \\ \vdots \\ d_i \\ \vdots \\ d_I \end{bmatrix}$$

where h and d are rainfall records of hourly and daily data matrices, respectively; i represents the index of daily data (i=1, 2, …, I) and I is the total number of rainy days; j represents the index of hourly data (j=1, 2, …, *24*). Therefore, hi,j means the jth hourly record corresponding to the ith daily record.

Construct a matrix W such that:

$$W = \begin{bmatrix} w_{1,1} & \cdots & w_{1,j} & \cdots & w_{1,24} \\ w_{i,1} & \cdots & w_{i,j} & \cdots & w_{i,24} \\ w_{I,1} & \cdots & w_{I,j} & \cdots & w_{I,24} \end{bmatrix}$$

where, wij is the weight of the jth hourly record over the corresponding daily record, which can be defined as:

$$wi,j = hi,j/di \qquad (1)$$

Step 2: Prepare vector $\boldsymbol{D'}$ (which is the transpose of D that represent the data containing the pool of k nearest neighbors):

$$D' = [d_1 \dots \quad d_i \dots \quad d_I]$$

The process starts by looking for the nearest neighbor to the elements of D in the elements of D'. The *K* nearest neighbors of *D* is found from the D' based on Euclidean distance (Danielsson, 1980). In this study, the nearest neighbors were selected based on the optimum window size approach (Alam and Elshorbagy, 2015).

Step 3: The selected nearest neighbor are captured in vector ***SD*** (with the same dimension as ***D***) based on the selected candidate neighbors from ***D'***, and for each data from ***SD***, formulate the corresponding proportions data series ***SW*** from ***W***:

$$SD_{wd} = \begin{bmatrix} sd_1 \\ \vdots \\ sd_i \\ \vdots \\ sd_I \end{bmatrix} \quad SW_{wd} = \begin{bmatrix} sw_{1,1} & \dots & sw_{1,j} & \dots & sw_{1,24} \\ sw_{i,1} & \dots & sw_{i,j} & \dots & sw_{i,24} \\ sw_{I,1} & \dots & sw_{I,j} & \dots & sw_{I,24} \end{bmatrix} \quad \forall wd=3,\ 5,\ 7,\dots,2n+1$$

where *wd* is the full window size and n is the number of windows considered (e.g. $\boldsymbol{SD_3}$ represents the vector capturing the nearest neighbors when the window size is set to 3 days; $\boldsymbol{SW_3}$ means the corresponding proportions of $\boldsymbol{SD_3}$) ; *swi,j* means the proportion of the *j*th hourly record corresponding to the *i*th daily record *sdi*. The final disaggregated results ***HD*** could be written as follows:

$$HD_{wd} = \begin{bmatrix} hd_{1,1} & \dots & hd_{1,j} & \dots & hd_{1,24} \\ hd_{i,1} & \dots & hd_{i,j} & \dots & hd_{i,24} \\ hd_{I,1} & \dots & hd_{I,j} & \dots & hd_{I,24} \end{bmatrix}$$

Where, $\boldsymbol{HD_{wd}}$ means the final disaggregated results based on the selected wd nearest neighbor; each element in ***HD*** is calculated by $hdi,j = swi,j \times di$. Therefore, for each window size there will be a final disaggregated results (HD).

Similarly, the sub-hourly disaggregation model was prepared by replacing the hourly and the daily matrices with the 5-min and hourly ones respectively.

4.3.2 K-NN model performance validation

Performance-validation was used to assess the performance of each window size. The criteria of performance-validation is to obtain the minimum of root-mean-square-error (RMSE) of the local extreme events which can be given as:

$$RMSE = \sqrt{\frac{\sum_{i=1}^{n} (X_{obs,y} - X_{model,y})^2}{Y}} \quad (2)$$

where, X_{obs} is observed annual maximum values and X_{model} is modelled annual maximum values at time Y given by:

$$X = \frac{(AMP_y\text{-}Minimum\ value)}{(Maximum\ value\text{-}Minimum\ value)} \quad (3)$$

where, $y = 1, 2, 3, \ldots,$ Y (total number of years in the time series).

The optimum window sized models were further tested using the Kolmogorov-Smirnov test (more details in next section) to confirm the model statistical simulation performance.

4.4 GEV Distribution and IDF Curves Development

The IDF curves for the baseline period and future projections were developed based on the generalized extreme value distribution which involves three parameters (scale, location and shape). GEV distribution combines Gumbel, Fréchet, and Weibull probability distributions. The cumulative probability distribution function for the GEV is given by:

$$F_{(x;\mu,\sigma,\xi)} = \exp\left[-\left(1 + \xi\frac{x-\mu}{\sigma}\right)^{-1/\xi}\right] \quad \forall \{1+[\xi(x-\mu)/\sigma] > 0\} \quad (4)$$

where, x is a random variable, μ is location, σ is scale and ξ is shape parameter. The GEV distribution converges to Gumbel, Fréchet, and Weibull distributions when the shape parameter $(\xi) = 0$, $\xi > 0$, and $\xi < 0$, respectively.

The location (μ), scale (σ) and shape (ξ), parameters of this distribution were estimated by the maximum likelihood estimation (MLE) method (Jenkinson 1955). Given an annual exceedance probability of R(X≤x), the return period is calculated by the reciprocal of R(X≤x).

$$\text{Return period } (T) = \frac{1}{R(X \leq x)} = \frac{1}{1-R(X>x)} = \frac{1}{1-F_{(x)}} \quad (5)$$

The extreme value theory that underlies the GEV distributions requires the assumption of stationarity of the climate. Most existing systems for water management and other infrastructure have been designed under the assumption that climate is stationary. Adjusted techniques are recommended when there are indications for non-stationarity (WMO, 2009). For that, R-based toolkit (Rextremes) was used to check the stationarity assumption and estimate the parameters of the GEV distribution.

The goodness-of-fit of the GEV distribution was evaluated by the Kolmogorov-Smirnov test. The K-S test was used to confirm whether the observed and simulated data belong to the same distribution. It is designed to test the null-hypothesis of no difference between observed and predicted distributions. The p-value reports the probability of incorrectly rejecting the null-hypothesis. A lower p-value (significance level 0.05) therefore suggests a stronger evidence for rejecting the null hypothesis.

CHAPTER 5: RESULTS AND DISCUSSION

5.1 Downscaling using LARS-WG 5.5

5.1.1 GCM Selection

In order to ensure the best simulation of the local scale data, two GCM's were selected out of five where the downscaled rainfall data from the five GCM's, namely MIROC5, HadGEM2-ES, INM-CM4, MRI-CGCM3 and CNRM-CM5, which have been evaluated based on the characteristics of the weather in the study area. For that, the comparison was made by considering another station located in the capital of the region, Salalah (20 km to the west of Tawi Atair) latitude 17.02° and longitude 54, as it is having the longest record of daily rainfall for the period 1950-2005. The baseline period was divided into two time slices in the process of calibration 1950-1977 and validation 1978-2005. Annual precipitation total, number of wet days, 95th percentile and daily maximum precipitation were considered in the comparison for the period 1978-2005. To further evaluate the performance of each GCM, the 2-tailed Kolmogorov-Smirnov goodness-of-fit test is applied to compare the probability distributions of the original and synthetic time series. Figure 8-10 and Table 5 summarize the results of the GCM selection comparison tests.

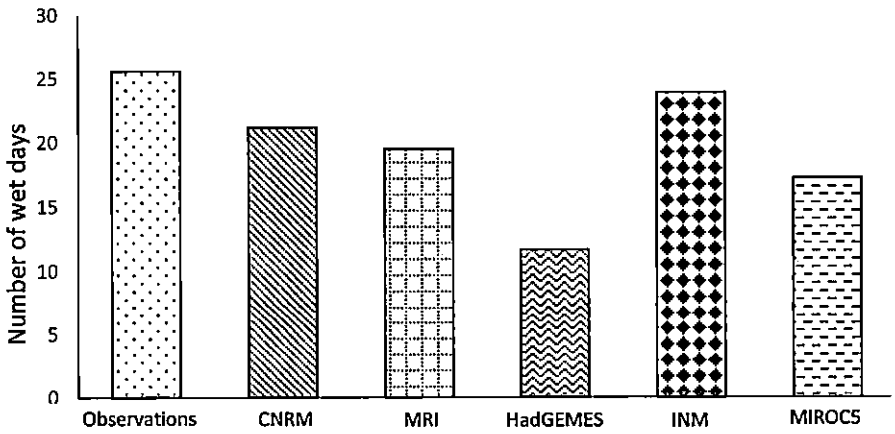

Figure 8 Comparison of the five GCMs with observations (Number of Wet Days)

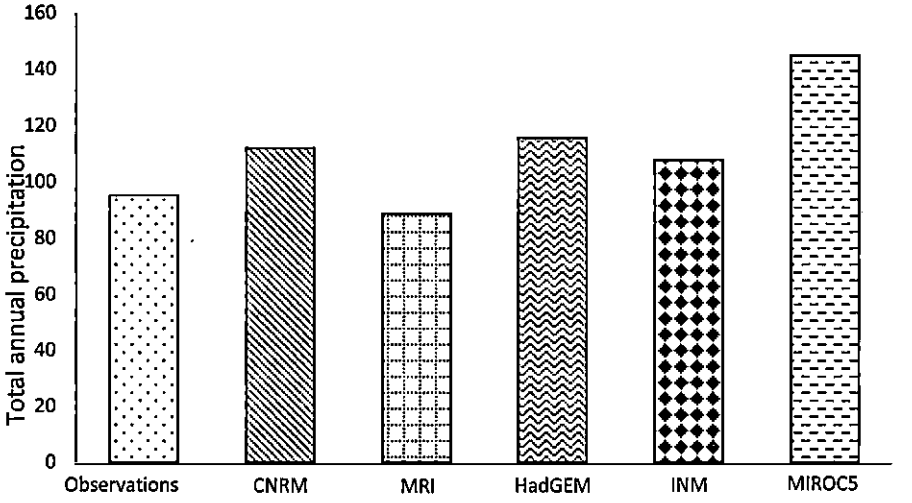

Figure 9 Comparison of the five GCMs with observations (Total Annual Rainfall mm)

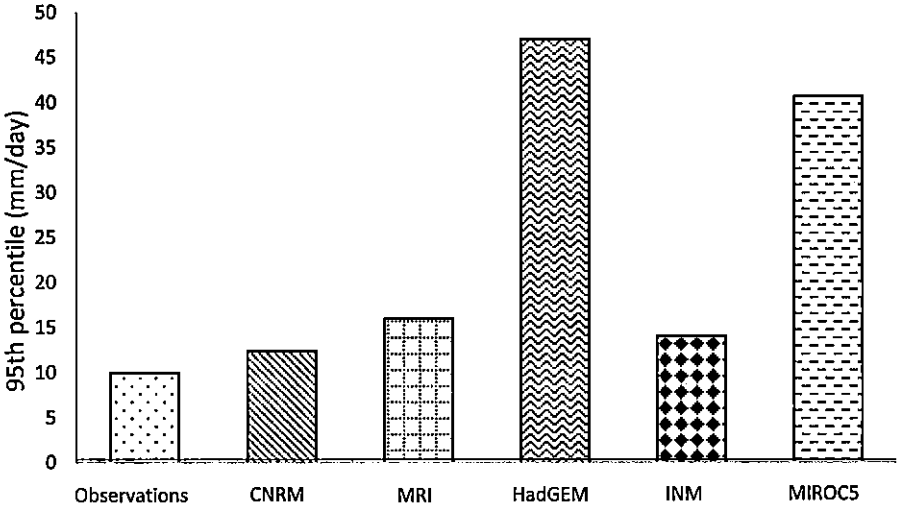

Figure 10 Comparison of the five GCMs with observations (95th Percentile)

Table 5: Kolmogorov-Smirnov goodness-of-fit

Modelling group	CMIP5 model name	p-value
Center for Climate System Research (University of Tokyo), National Institute for Environmental Studies and Frontier	MIROC5	0.011
Hadley Centre for Climate Prediction and Research, UK	HadGEM2-ES	0.001
Institute for Numerical Mathematics, Russia	INM-CM4	0.000
Meteo-France/Centre National de Recherches Meteorologiques, France	CNRM-CM5	**0.357**
Meteorological Research Institute, Japan	MRI-CGCM3	**0.051**

Among the five GCM's, MRI-CGCM3, INM-CM4 and CNRM-CM5 have shown better performance than other GCM's. The K-S test confirmed two GCMs, MRI-CGCM3 and CNRM-CM5 with p-value greater than 0.05 and therefore were selected to generate the future projection for the study area, Tawi Atair. The failure of INM-CM4 to pass the K-S test is due to an event above 95th percentile which could have resulted in considerable mismatch in the cumulative distributions.

5.1.2 Calibration and Validation of Lars-WG

Before beginning the downscaling process of the two selected GCM's to the local scale of Tawi Atair station, the Lars-WG performance was evaluated by calibration of the site observations to obtain the site parameters (wet and dry series lengths, rainfall amounts by month, ... etc) required to generate the synthetic rainfall data having the same statistical characteristics as the original observed rainfall data. The simulated and observed results were then validated by comparing several weather characteristics of both results. In this case, the mean monthly rainfall with standard deviations (SD), the 95th percentile and the monthly maximum rainfall of the observed vs the simulated data were considered in the comparison test for the baseline period (1993-2009). The results are shown in Figures 11-13.

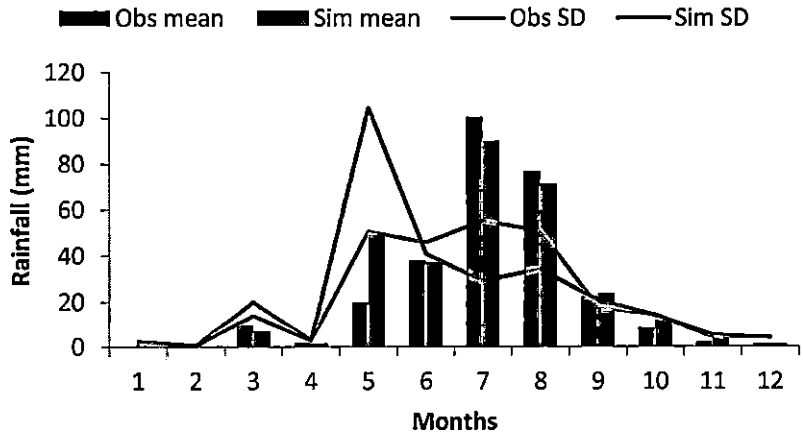

Figure 11 Comparison of observed and LARS-WG simulated mean monthly rainfall with SD at Tawi Atair station for the baseline period (1993-2009).

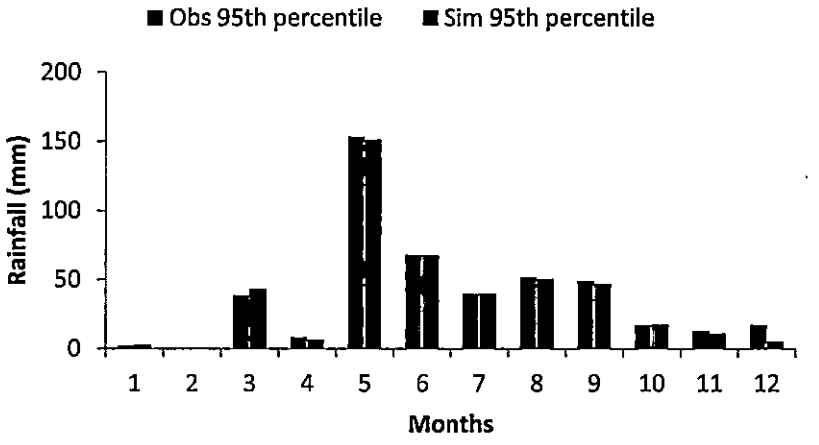

Figure 12 Comparison of observed and LARS-WG simulated 95th percentile precipitation at Tawi Atair station for the baseline period (1993-2009).

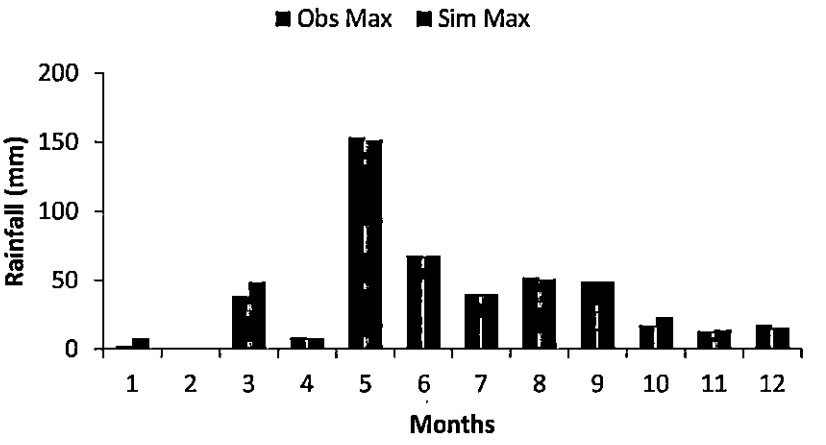

Figure 13 Comparison of observed and LARS-WG simulated monthly maximum precipitation at Tawi Atair station for the baseline period (1993-2009).

The Lars-WG overall performance was good especially in simulating the 95th percentile and the monthly maximum rainfalls as shown in Figure 12 & 13. But when considering the simulation of the mean monthly rainfall Figure 11, the weather generator seems to overestimate the mean monthly in May and underestimate it in July and August. However, knowing that this study is more focused on the extreme rainfall events, this deficiency will not have a significant impact on the final goal.

5.2 K-Nearest Neighbor Disaggregation

A model for daily to hourly disaggregation was developed considering 30 window sizes to disaggregate the observed daily data and obtain the optimum window size which should have the minimum RMSE value. The window size (wd) represents the day to be disaggregated plus a number of days before and after it, i.e. the first window size is actually a day plus 1 day before and another after which corresponds to 3 days. Therefore if n = number of windows {1, 2, 3,... , 30}, then the size wd= 1+2n.

An excel spread sheet was developed to perform the K-NN disaggregation. A macro VBA program was developed to automatically change the window size and extract the RMSE value for each window size (Appendix A). If a certain window size does not find a rainy day (at least one nearest neighbor) then it moves to the next window size until one nearest neighbor is found. Therefore, for every daily record of the observed baseline data, a nearest neighbor will be generated for every window size considered from all the years excluding the day which is required to be disaggregated to avoid self-simulation (Alam and Elshorbagy, 2015).

Figure 14 shows the performance of each window size and the optimum window size was found to be 28 days (57 days of full window). The K-S test result for the obtained optimum window also confirms the K-NN model with p-value of 0.348. The K-S test comparison results for the hourly disaggregation model are shown in Figure 15 and 16.

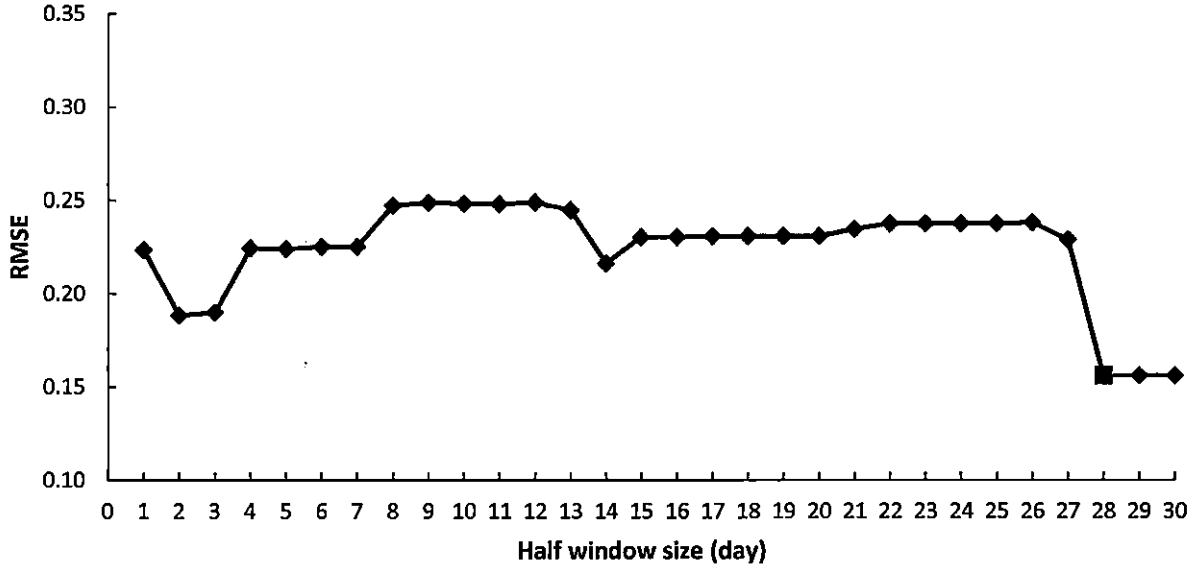

Figure 14 Window size performance for K-NN hourly disaggregation

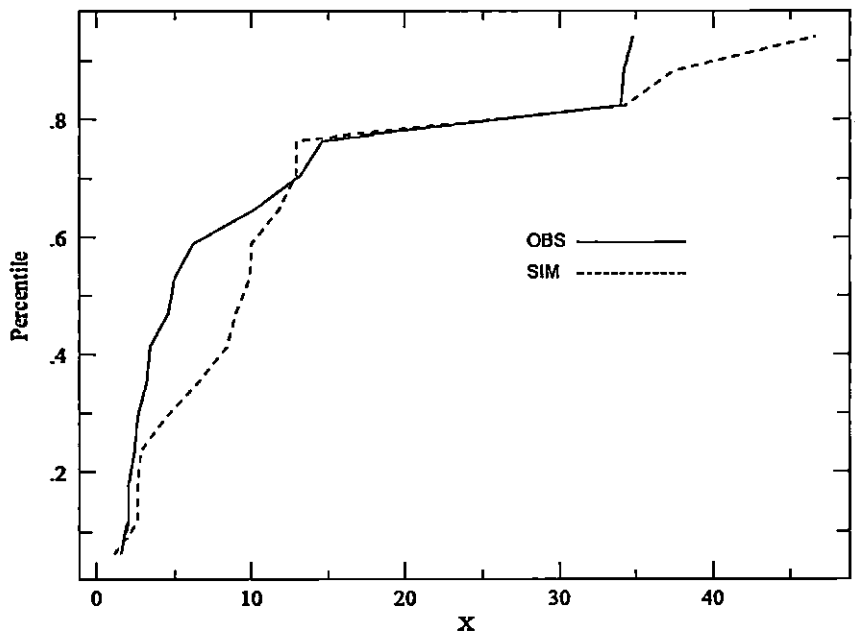

Figure 15 K-S test comparison percentile plot (hourly disaggregation model)

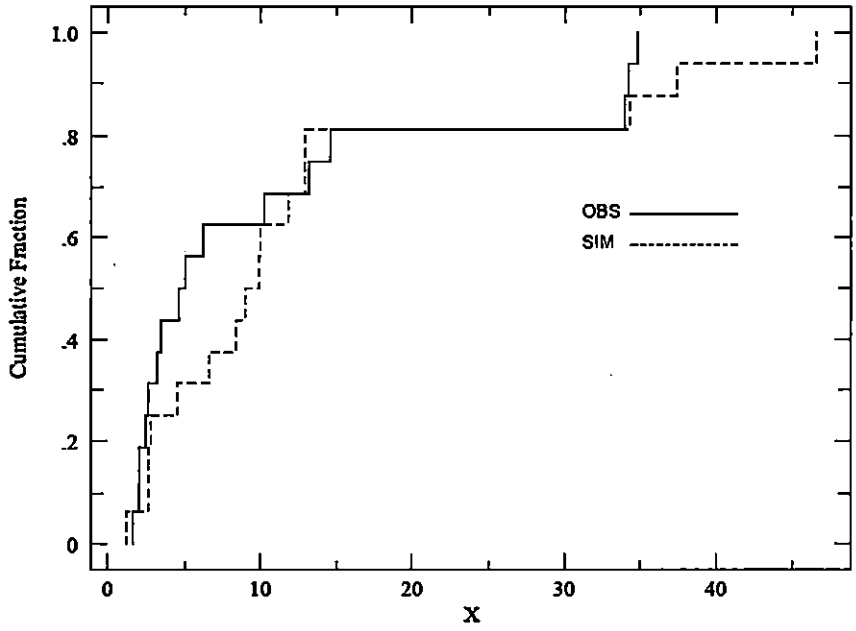

Figure 16 K-S test comparison cumulative fraction plot (hourly disaggregation model)

Similarly, for the 5-min disaggregation, the hourly model was modified to execute the 5-min disaggregation. In this model, the window size (wh) is expressed in hours. In total, 120 window sizes (full window with 241 hours) were considered when finding the optimum window size. The performance of each window size is shown in Figure 17. The optimum window size was found to be 90 hours (181 hours of full window). The K-S test result for the obtained optimum window also confirms the K-NN model with p-value of 0.912. The K-S test comparison results for the sub-hourly disaggregation model are shown in Figure 18 and 19.

Figure 17 Window size performance for K-NN Sub-hourly disaggregation

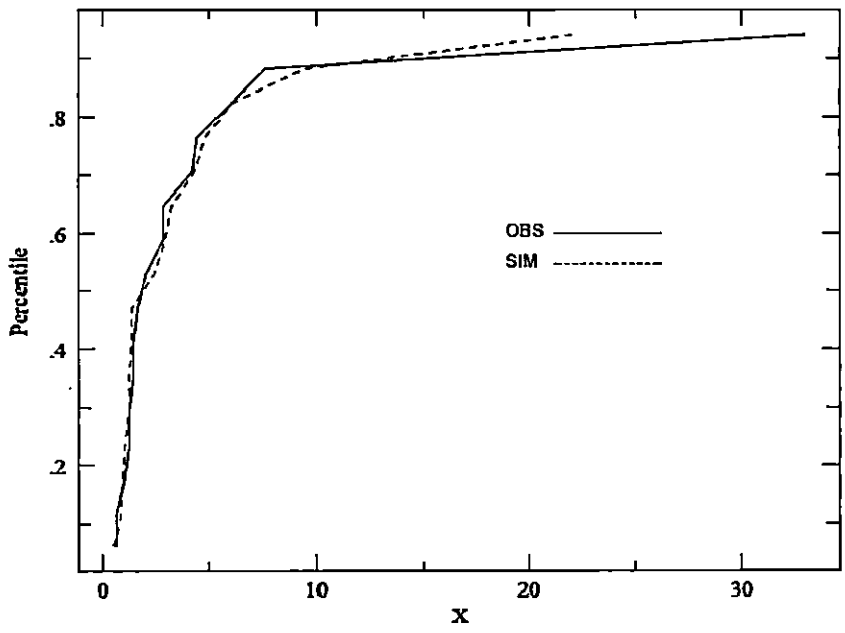

Figure 18 K-S test comparison percentile plot (sub-hourly disaggregation model)

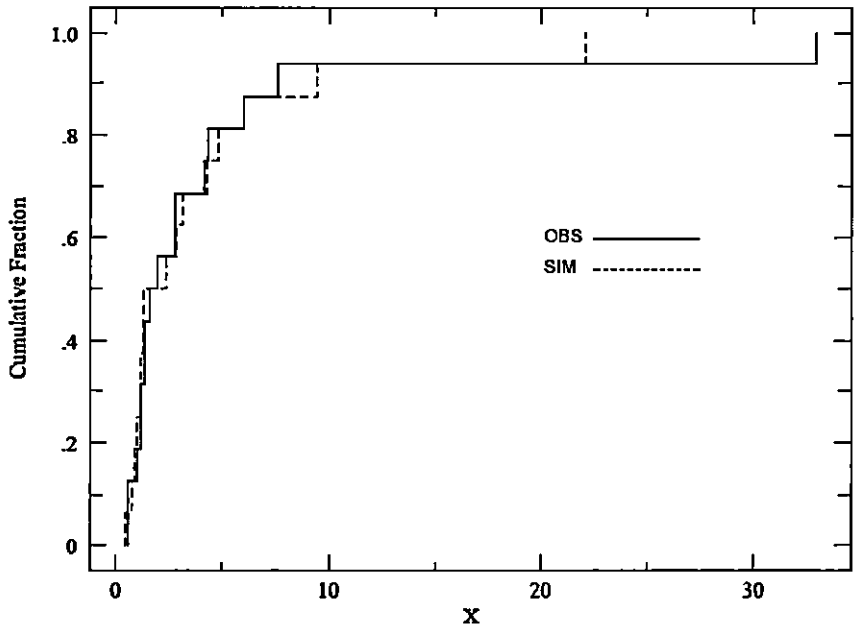

Figure 19 K-S test comparison percentile plot (sub-hourly disaggregation model)

The above two models of disaggregation, were utilized to disaggregate the future downscaled GCM daily data into hours and 5-min time series.

5.3 IDF curves and Future Projections

5.3.1 Historical IDF curves

The historical IDF curves were constructed by fitting the GEV distribution function to the Annual Maximum Rainfalls (AMR's) of the baseline period using the R-extreme toolkit. The goodness-of-fit was evaluated using Kolmogorov-Smirnov test with 5% significance level. The resulting GEV parameters for the specified durations (5-min, 15-min, ... 24-hrs) and the associated p-values for the K-S test are shown in Table 6. Figure 20 shows the probability-probability plots and Quantile-Quantile plots of the empirical to the modelled results. The p-value results and the regression lines confirm the goodness-of-fit using the GEV distribution.

Table 6 GEV parameters for different durations (Baseline Period)

		Duration (minutes)							
		5	15	30	60	120	360	720	1440
GEV Parameters	Mu	18.233	10.308	7.029	4.232	2.666	1.555	1.012	0.641
	Sigma	17.299	10.023	7.731	4.535	2.510	1.225	0.788	0.439
	Xi	0.187	0.317	0.322	0.424	0.489	0.511	0.473	0.546
K-S test	p-value	0.922	0.992	0.935	0.856	0.887	0.863	0.750	0.843

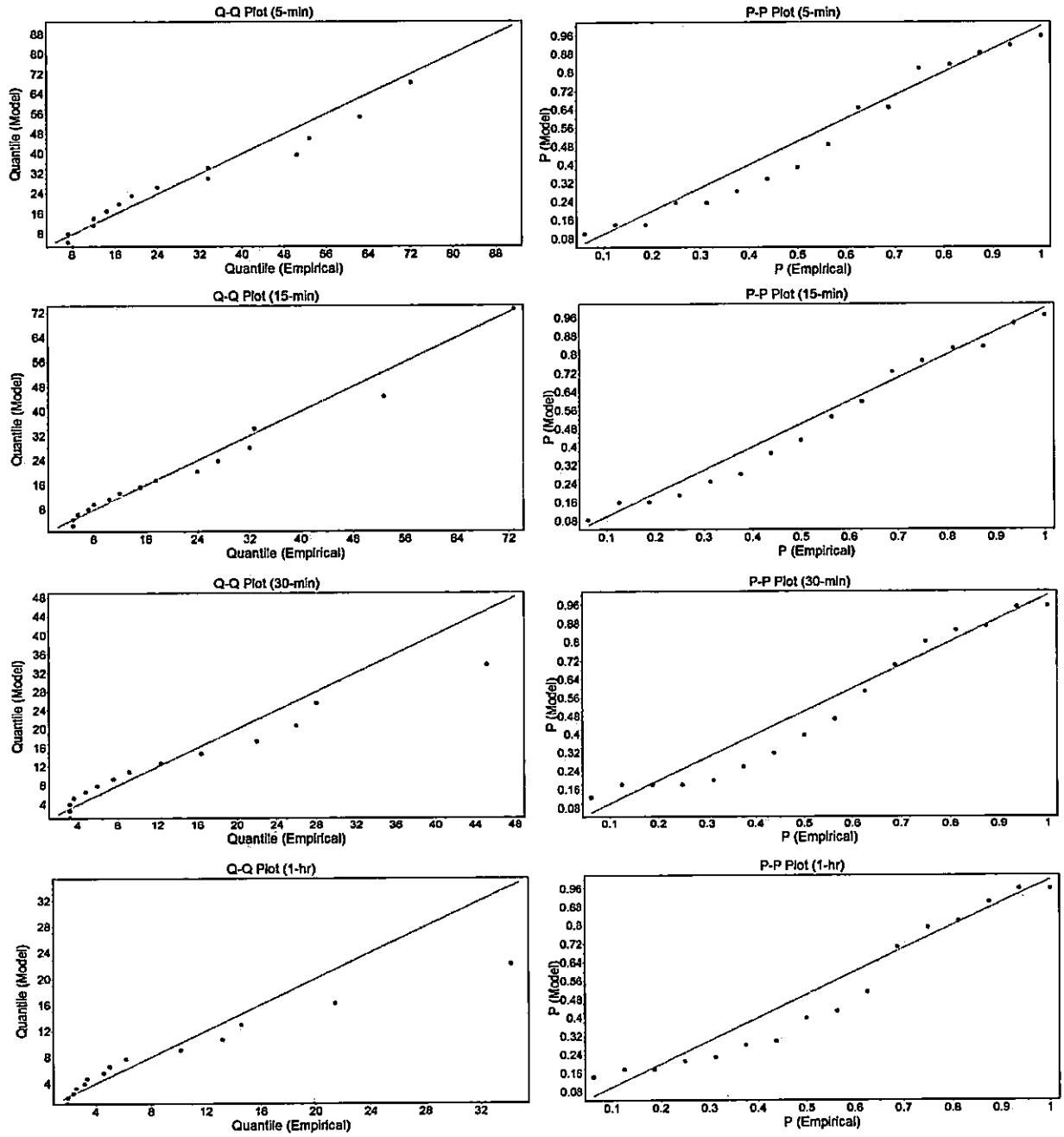

Figure 20 Q-Q and P-P plots for the GEV fitting of the historical observations (1998-2015)

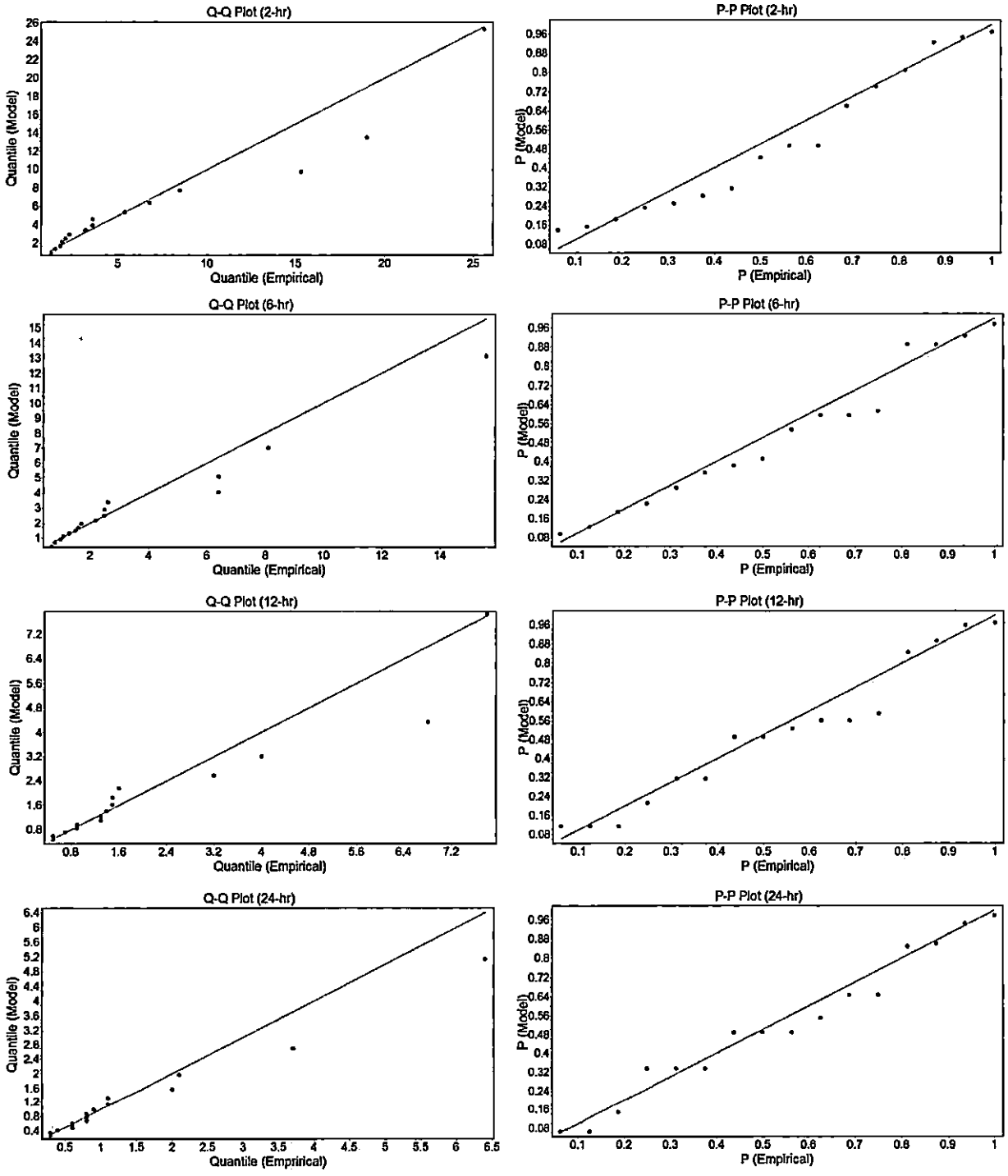

Figure 20 Q-Q and P-P plots for the GEV fitting of the historical observations (1998-2015), Continued

5.3.2 Future IDF curves

Similarly, the Annual Maximum Rainfall (AMR) for downscaled-disaggregated future projections for the two GCM's, two RCP's and two future time periods were obtained and analyzed by R-extreme toolkit. The annual maximum rainfalls were fitted to the GEV distributions to obtain the GEV parameters necessary to calculate the return levels for the specified return periods.

Future projections of IDF were constructed by comprising the AMR's of the specific future period plus the historical record. For example, the 2080-2099 period comprises the AMR's of the baseline period, the 2040-2059 and the 2080-2099 periods in the GEV fitting process.

Figures 21-28 shows the Intensity-Return Period plots obtained for all scenarios under each duration considered in the analysis. The average of all scenarios divided into three time slices, baseline period, 2040-2059 & 2080-2099 is shown in Table 7 and Figure 29. Appendix (B) Table B-1 contains all of the individual scenarios IDF results in a table format.

The percentage of change from the historical IDF curves to the future ones differs depending upon the duration, return period and time slice. The changes in the rainfall intensities increase from longer duration storms to shorter ones and from smaller return periods to larger ones. In general, when considering the average of all scenarios considered in producing the future IDF curves (Table 7), the rainfall intensities are increasing towards the end of 21st century. This is clearly apparent in the short duration storms (5min-30-min). Storms with high durations did not show a consistent behavior with a decrease towards the end of the 21st century. This might be supported with the findings of Al-Habsi et al. (2014) that the total annual rainfall is expected to decrease in the region with a rate of 0.194mm/year (19.4mm/100 years) and that the contribution to the total annual will be dominated by the extreme short duration's storms. In Qatar, Al Mamoon et al. (2016) investigated the sensitivity of the design rainfall of 24-hr annual maximum rainfall to climate change scenarios represented by two GCMs under SRES A2 family over two future periods, 2040-2069 and 2080-2099. The change in 24-hr AMR projected over 2040-2069 were not significant but 2080-2099 projection have shown a significant increase.

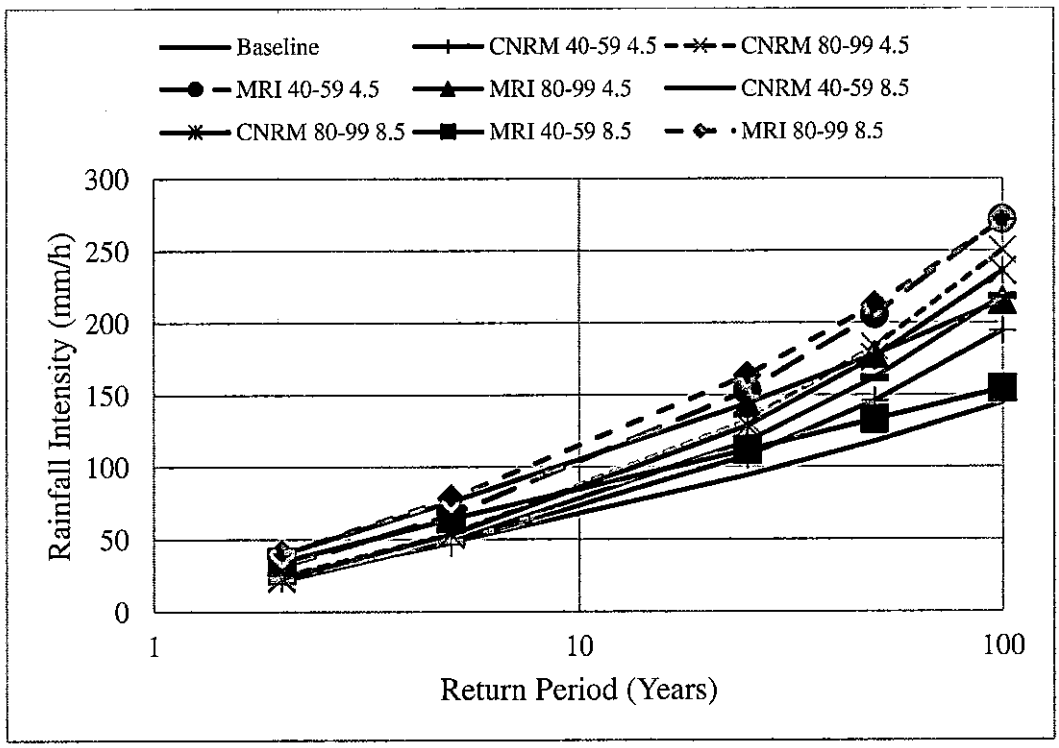

Figure 21 Intensity-Duration plot Under All scenarios (5-min)

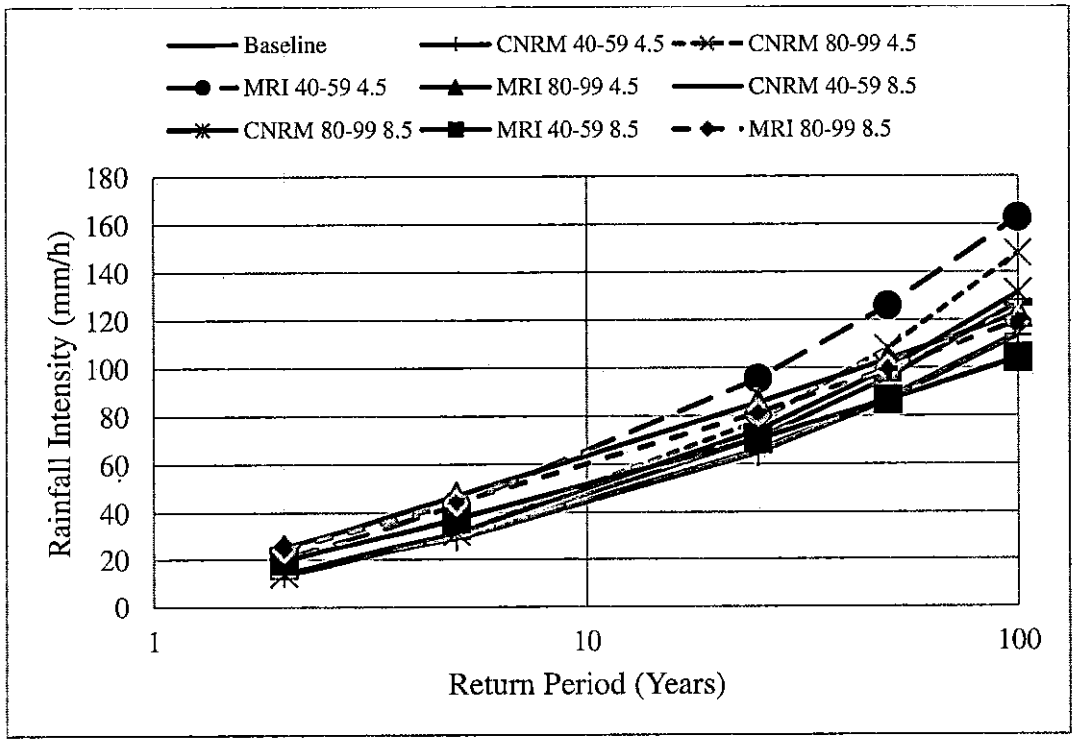

Figure 22 Intensity-Duration plot Under All scenarios (15-min)

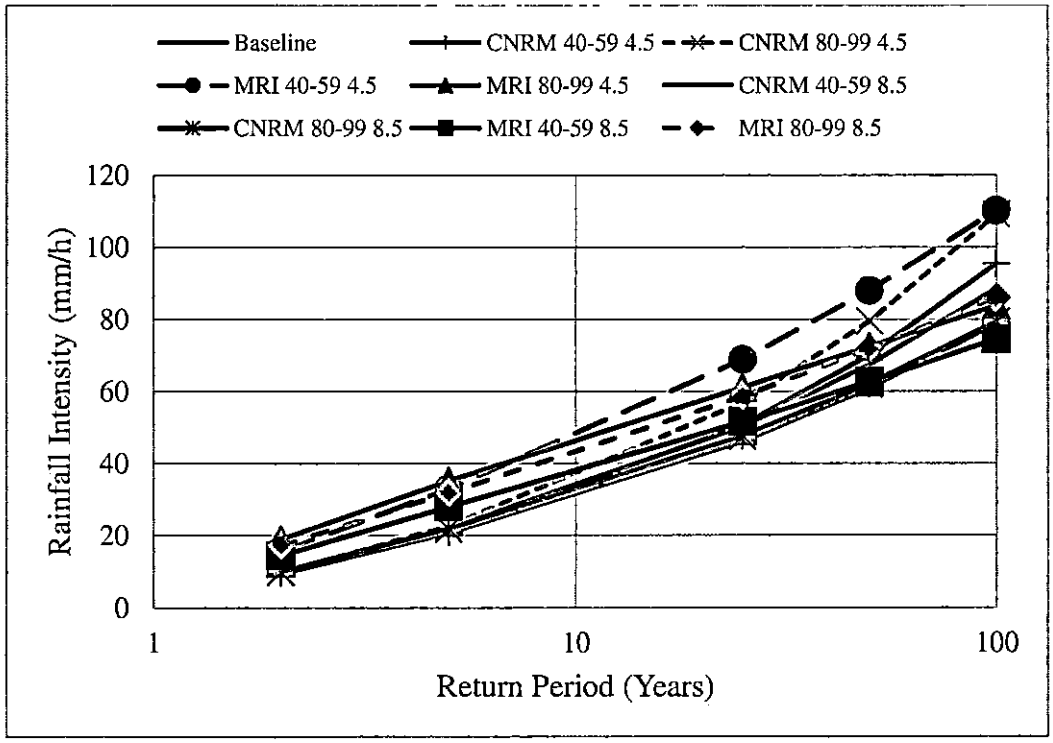

Figure 23 Intensity-Duration plot Under All scenarios (30-min)

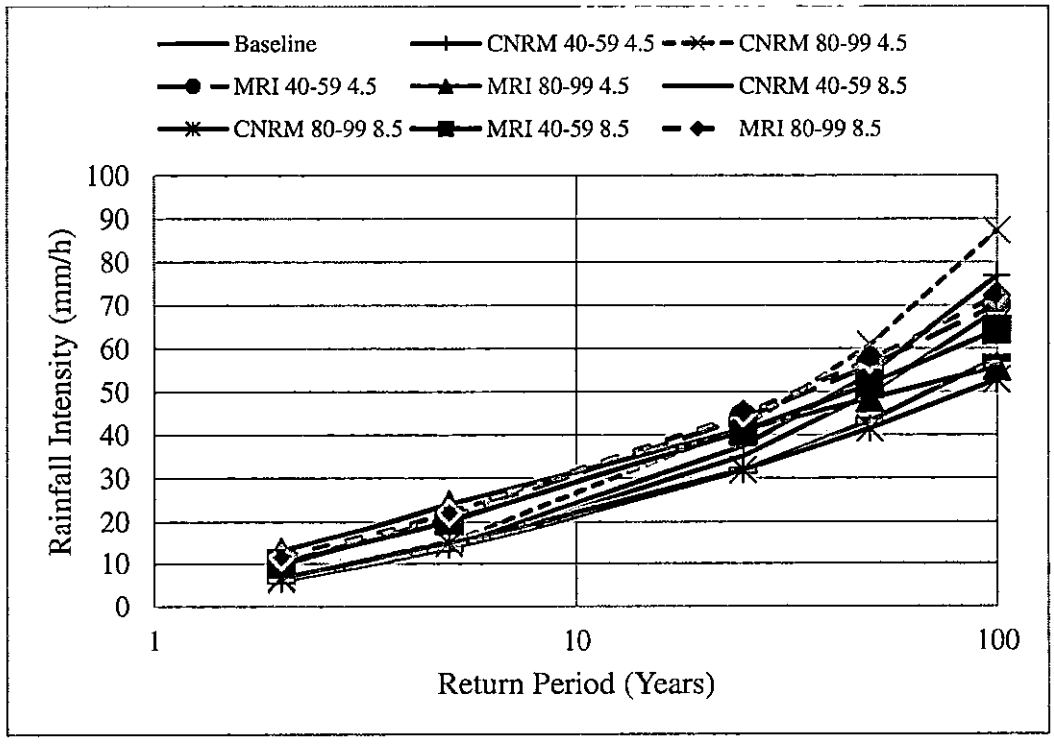

Figure 24 Intensity-Duration plot Under All scenarios (1-hr)

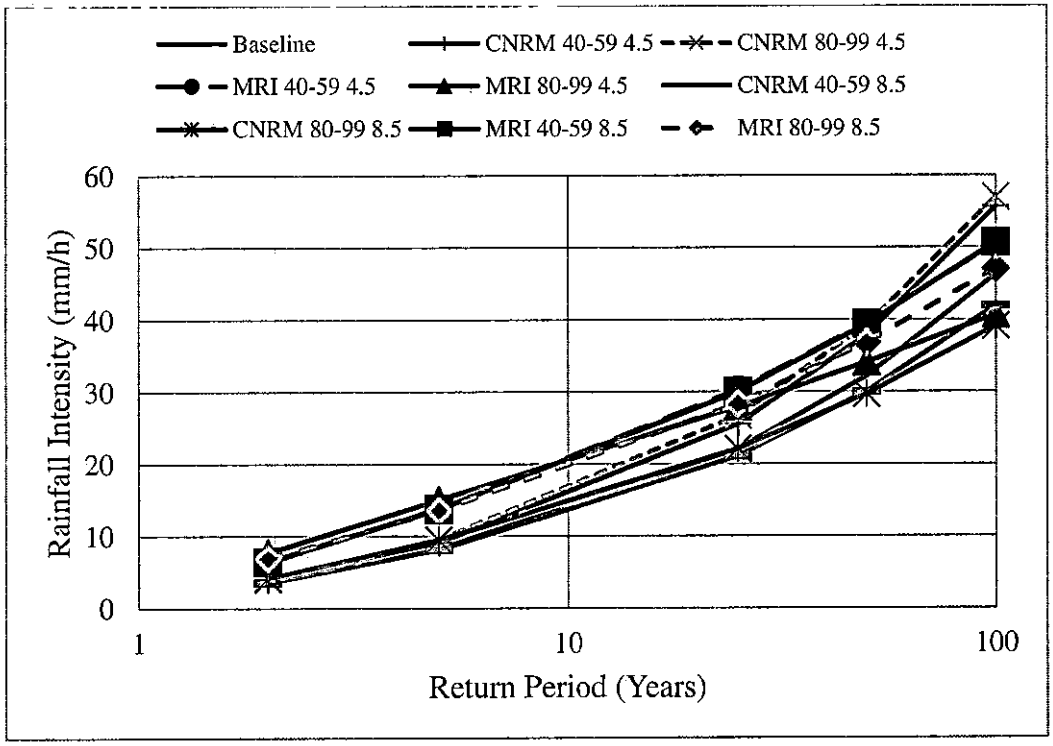

Figure 25 Intensity-Duration plot Under All scenarios (2-hr)

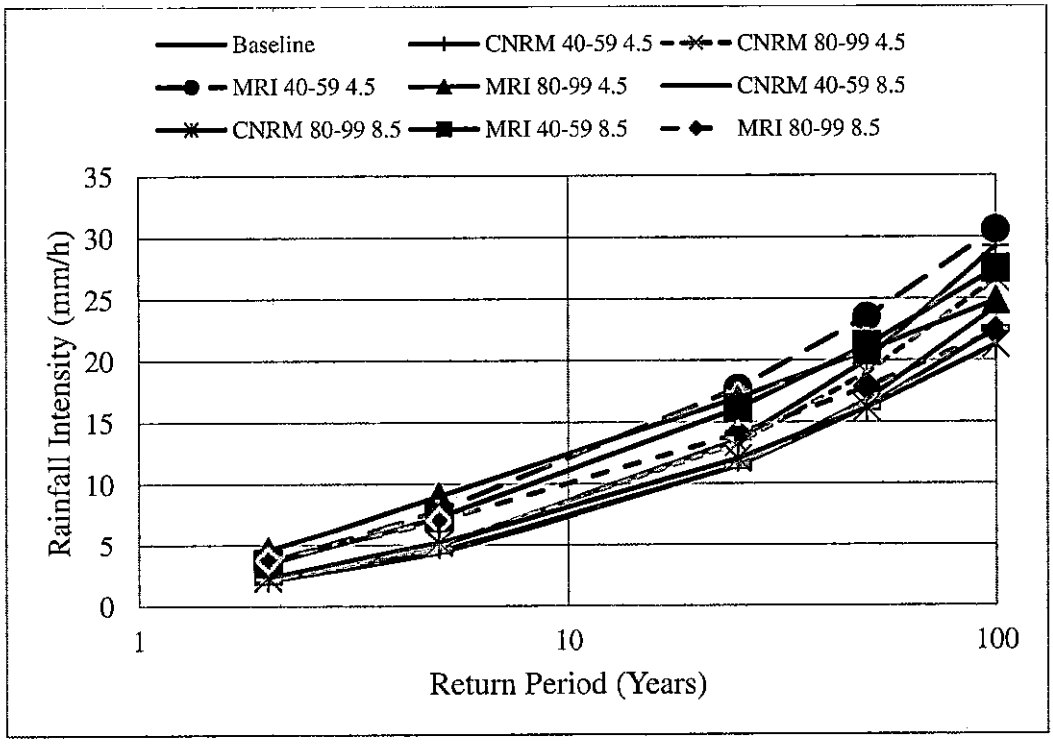

Figure 26 Intensity-Duration plot Under All scenarios (6-hr)

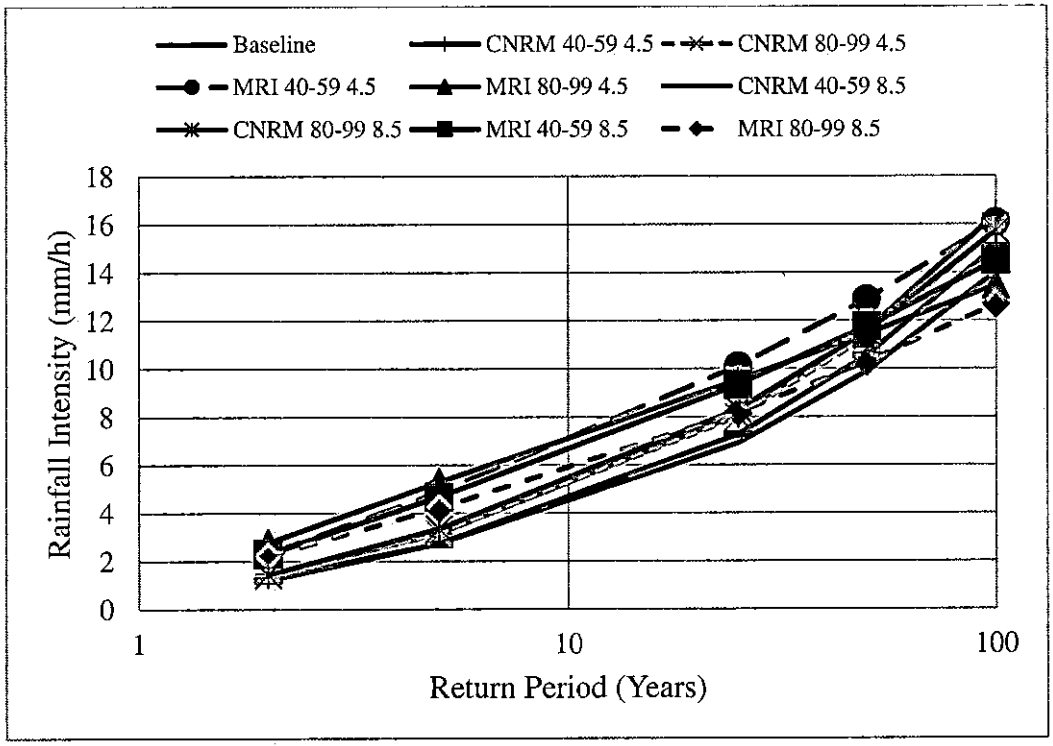

Figure 27 Intensity-Duration plot Under All scenarios (12-hr)

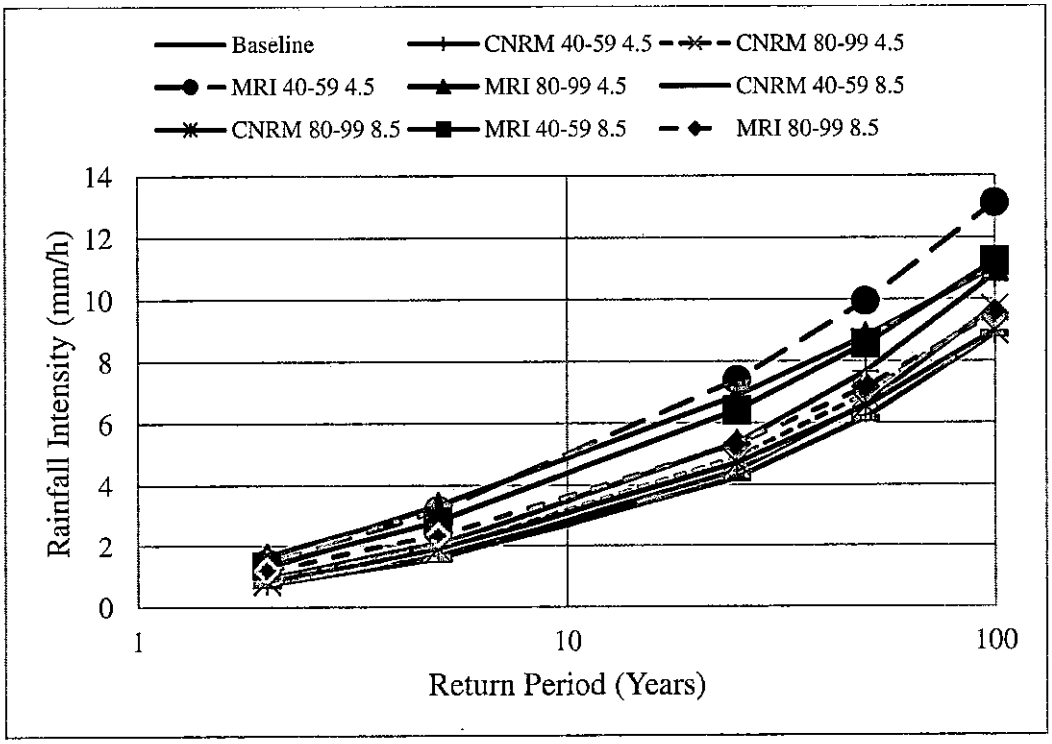

Figure 28 Intensity-Duration plot Under All scenarios (24-hr)

Table 7 Average of all GCM's and RCP's over three time periods

	Baseline 1998-2015					2040-2059					2080-2099				
	2-yr	5-yr	25-yr	50-yr	100-yr	2-yr	5-yr	25-yr	50-yr	100-yr	2-yr	5-yr	25-yr	50-yr	100-yr
5-min	25	48	94	118	144	28	57	122	161	209	32	65	142	187	243
15-min	14	30	66	88	114	17	35	75	99	127	19	39	80	103	130
30-min	10	22	50	67	89	12	26	54	70	90	14	28	56	71	90
1-hr	6	14	35	50	69	8	17	38	51	67	9	19	40	52	67
2-hr	4	8	22	32	46	5	11	27	37	50	6	12	26	35	46
6-hr	2	4	11	17	24	3	6	15	20	27	3	7	14	18	24
12-hr	1	3	7	10	14	2	4	9	12	15	2	4	8	11	14
24-hr	1	2	4	7	10	1	2	6	8	11	1	2	5	7	10

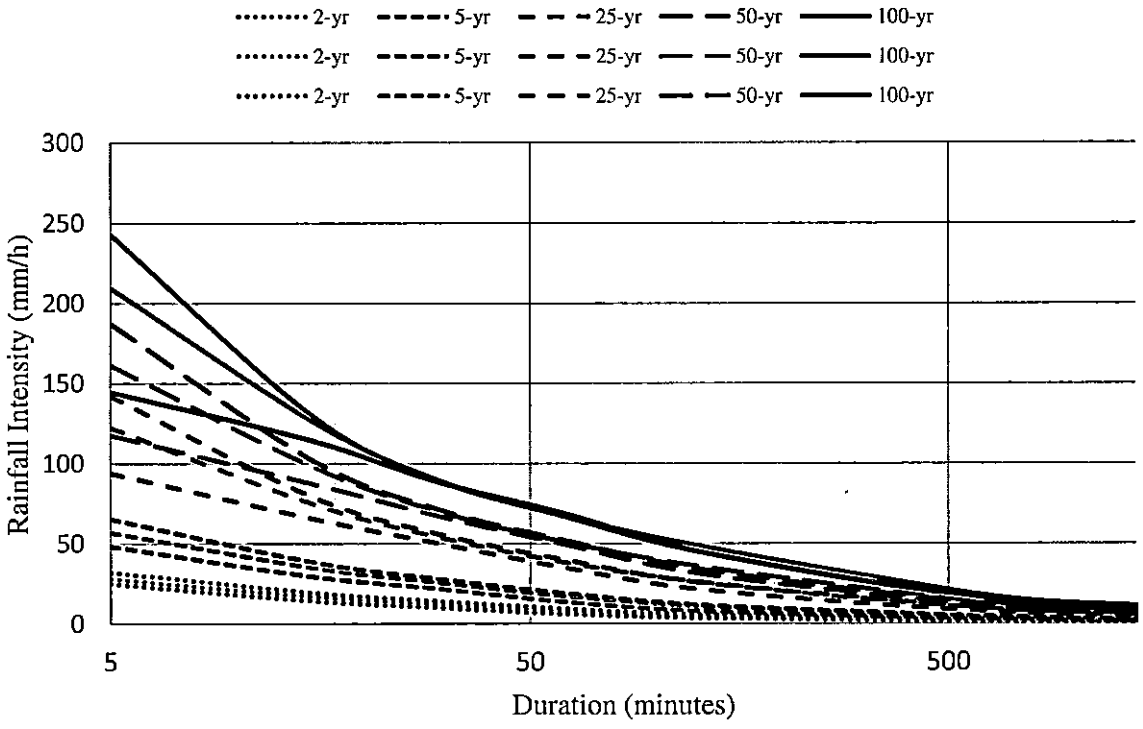

Figure 29 Average of all GCM's and RCP's over three time periods, baseline(black), 2040-2059 (blue) & 2080-2099 (red) IDF Curves

5.4 Variations Analysis

The obtained results in this study based on two GCM's and two RCP's for two future periods are clearly variable in the IDF curves generated for Tawi Atair. The selection of GCM, the radiative forcing scenario and the downscaling/disaggregation methods play a major role in producing such variability. GCMs vary owing to the horizontal resolution and their modeling nature. The RCPs represent different GHG's emission and concentration scenarios and therefore may produce different IDF futures.

5.4.1 Variations due to GCM and RCP

Figure 30 a- e illustrates the variability attributed to RCP selection when fixing the GCM and time slice for the different return periods. The effect of changing the RCP in the CNRM is very small in both time slice and return periods. Whereas MRI has shown a relatively greater response to RCP change. For example, the 5-min 100-yr return period storm during 2080-2099 for CNRM has a range of 236-250 mm/hr compared to 215-271 mm/hr for the MRI due to RCP change.

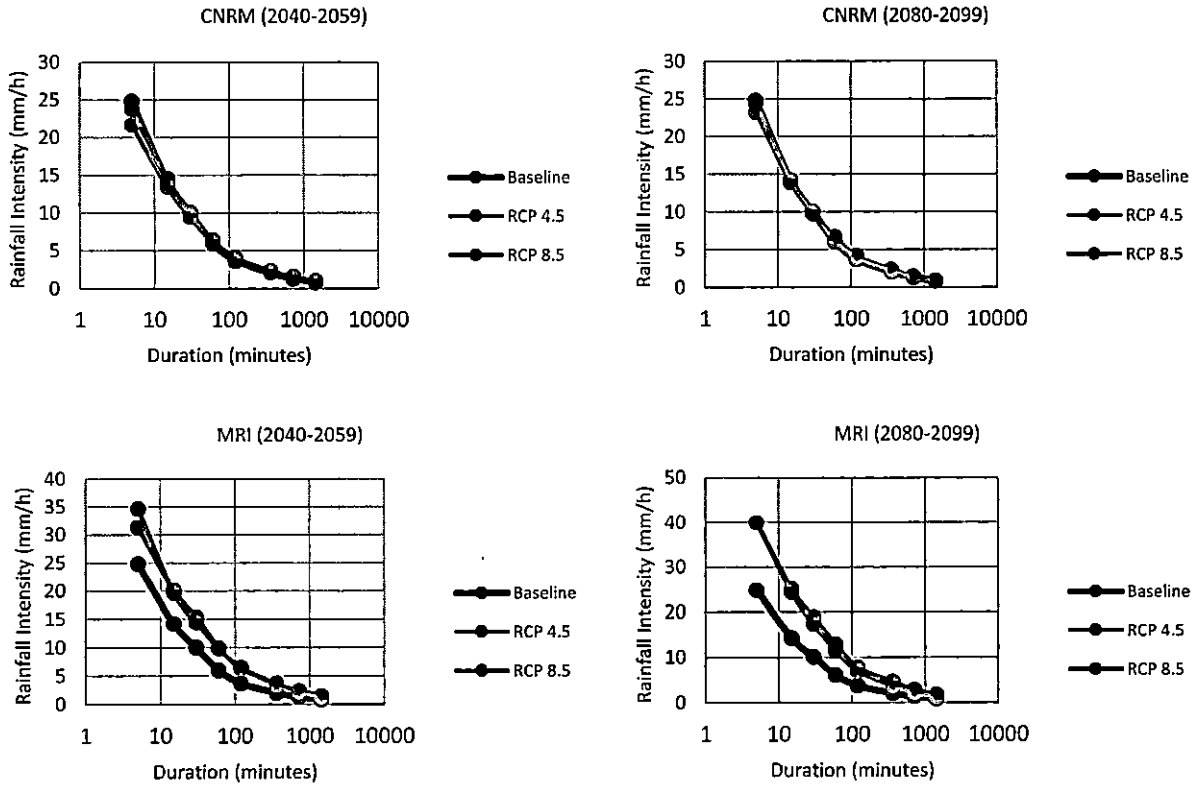

Figure 30 (a) Variability from RCP selection under two GCMs and two time slices (2-yr return period)

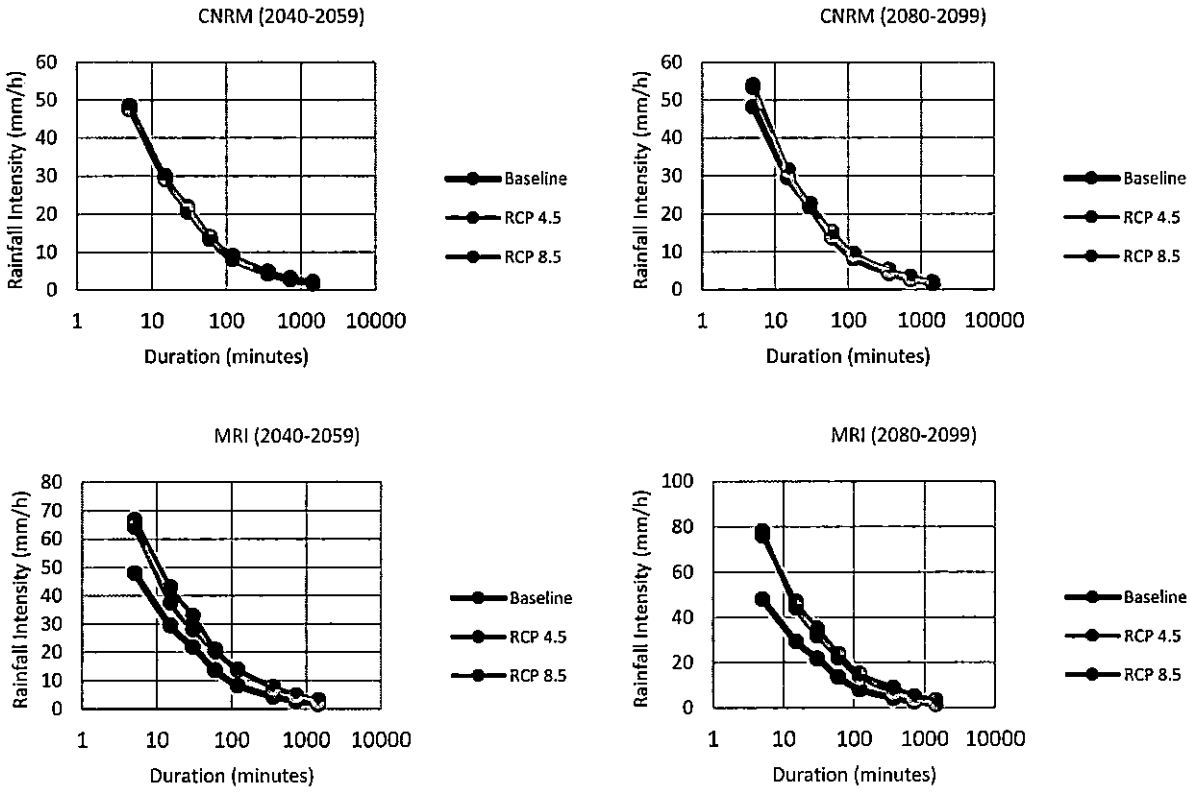

Figure 30 (b) Variability from RCP selection under two GCMs and two time slices (5-yr return period)

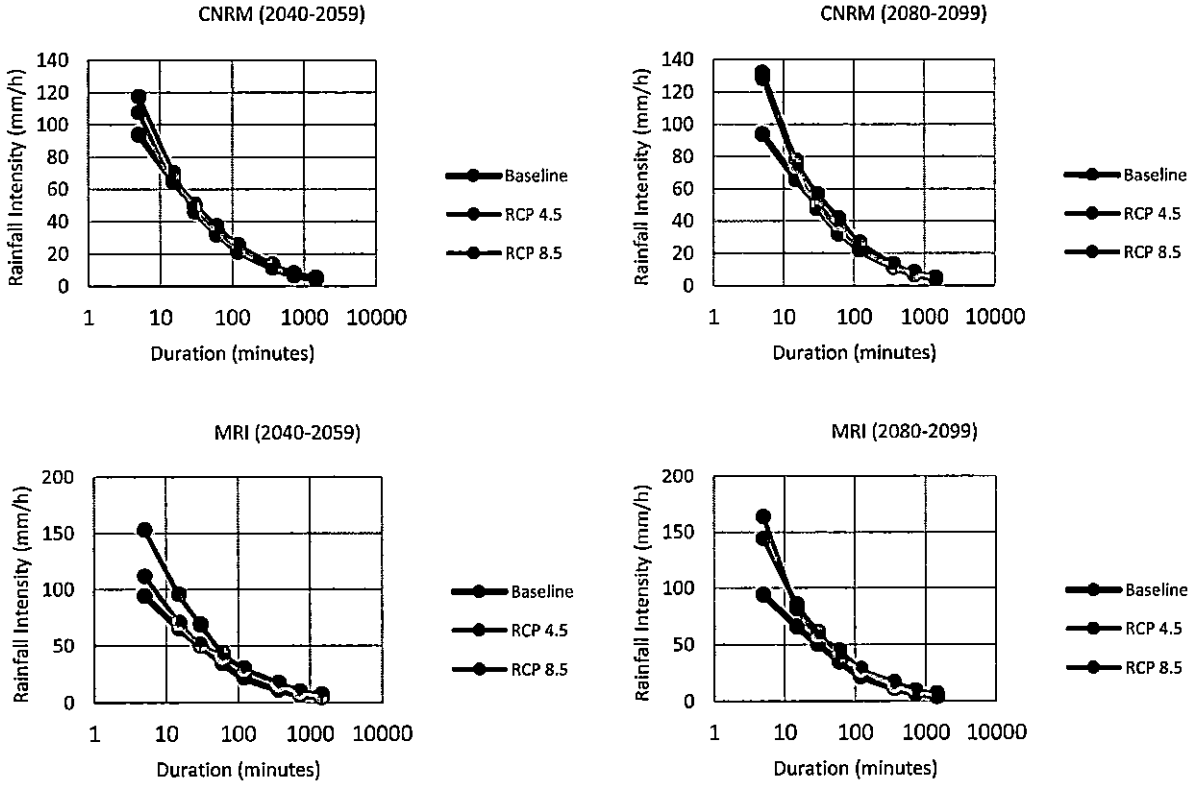

Figure 30 (c) Variability from RCP selection under two GCMs and two time slices (25-yr return period)

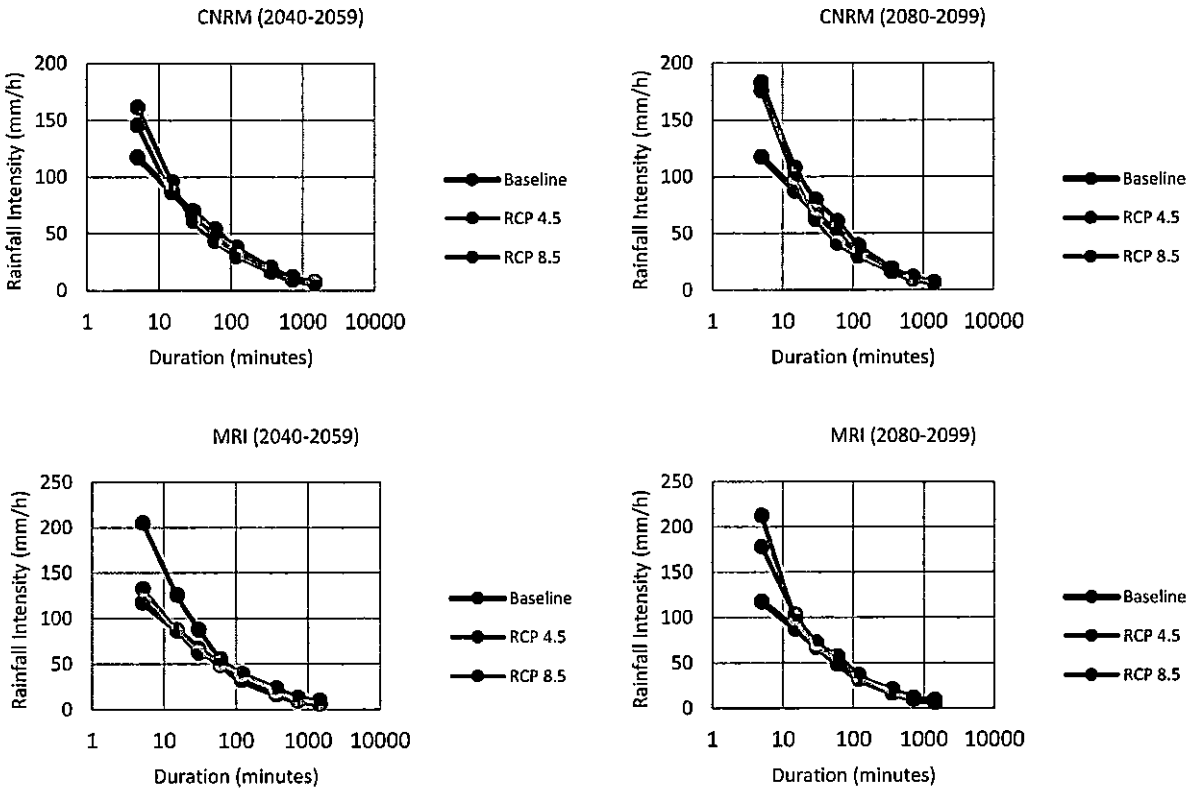

Figure 30 (d) Variability from RCP selection under two GCMs and two time slices (50-yr return period)

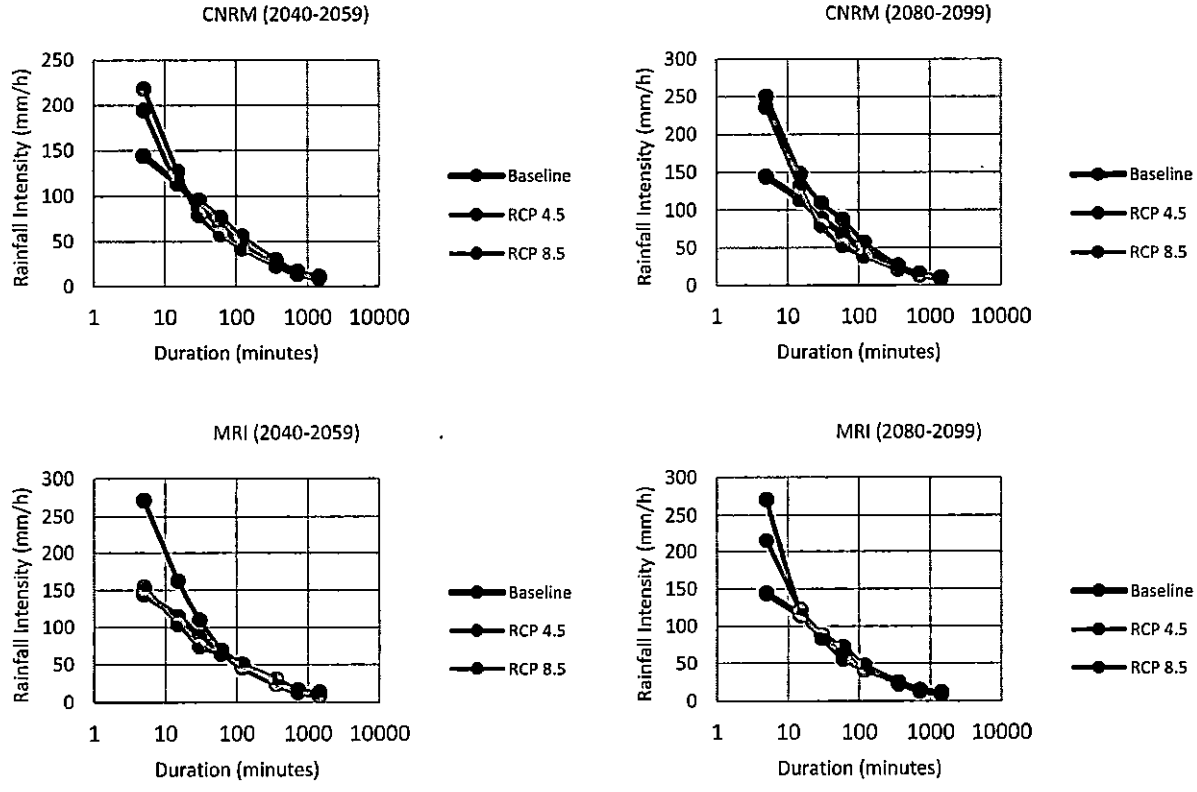

Figure 30 (e) Variability from RCP selection under two GCMs and two time slices (100-yr return period)

The GCM selection has also contributed to the variability in results as shown in Figure 31 a- e for all return periods. For example, by fixing the RCP to 8.5, the intensity level of MRI 5-min storm, 2-yr return period during 2080-2099 is 40 mm/hr compared to 23 mm/hr for the CNRM. Similarly for the 100-yr return period, the 2040-2059 MRI, 15-min rainfall intensity under RCP 4.5 is 163 mm/hr compared to 113 mm/hr for the CNRM.

It can be concluded from the generated plots that the variations due to GCM selection is more compared to the RCP change.

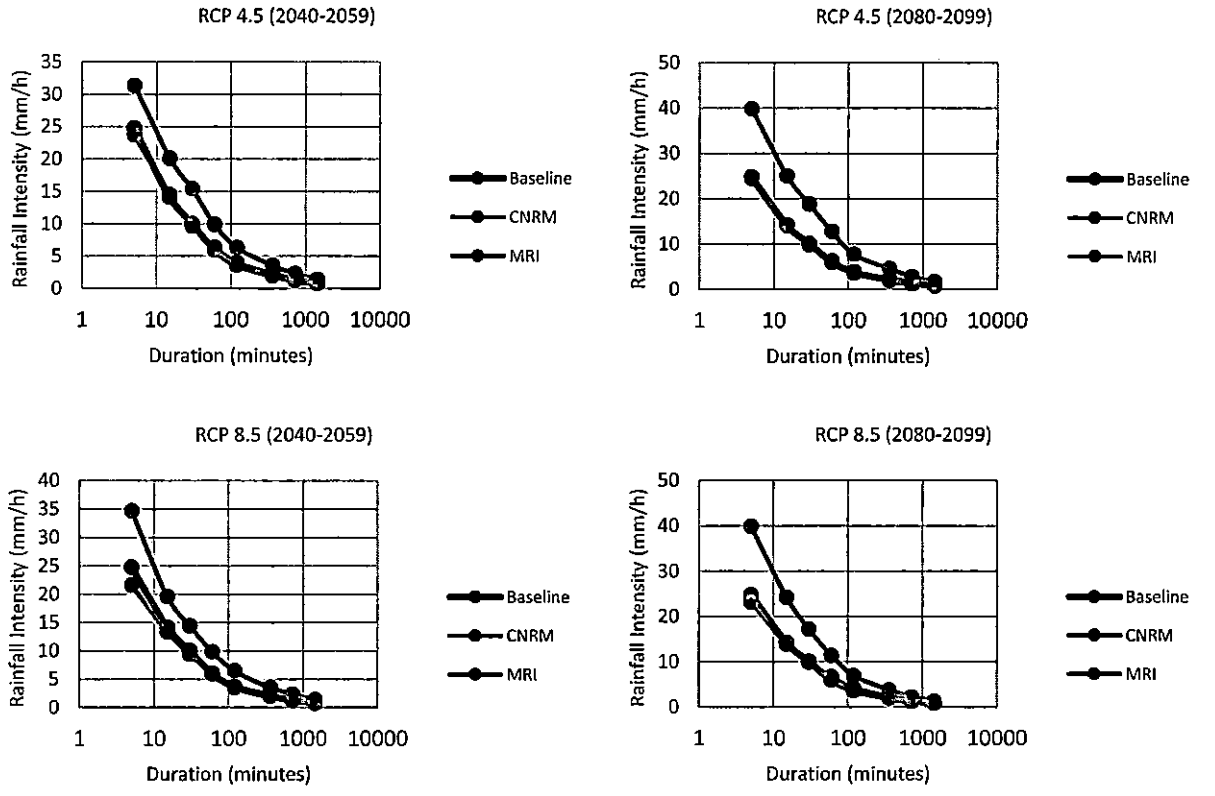

Figure 31 (a) Variability from GCM selection under two RCPs and two time slices (2-yr return period)

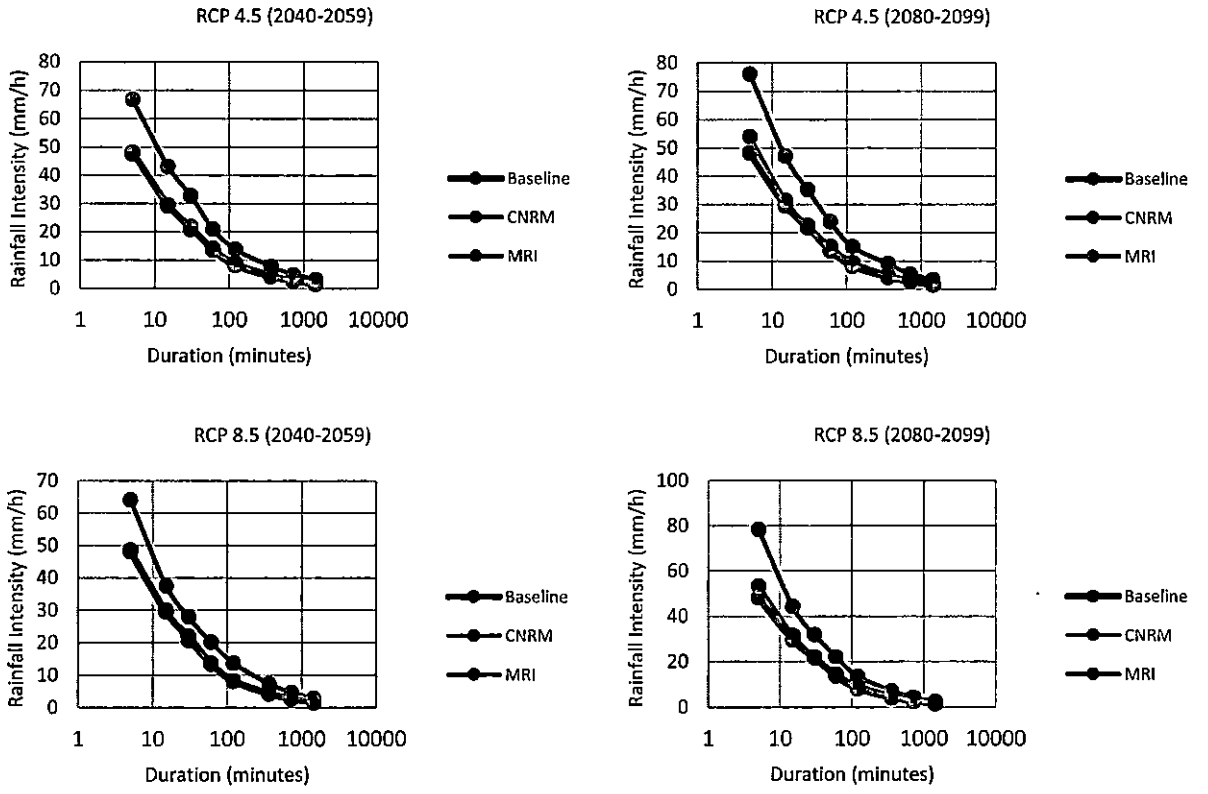

Figure 31 (b) Variability from GCM selection under two RCPs and two time slices (5-yr return period)

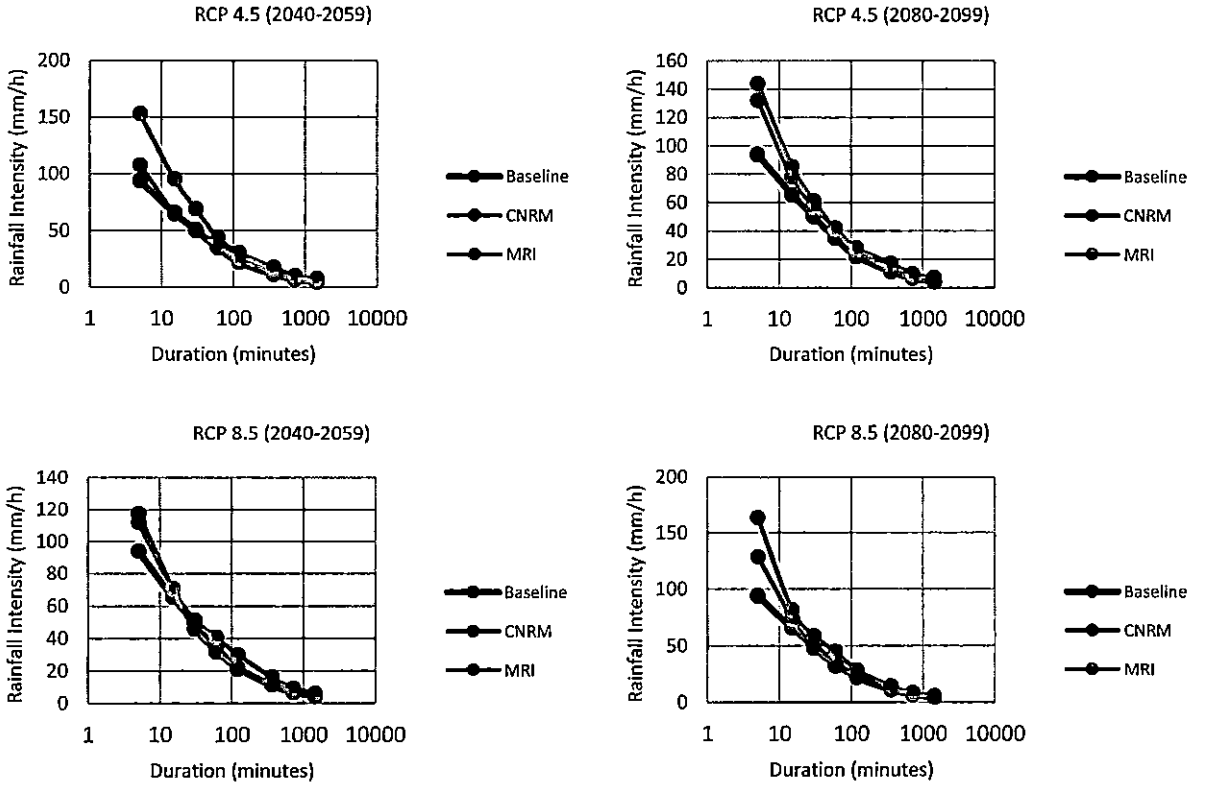

Figure 31 (c) Variability from GCM selection under two RCPs and two time slices (25-yr return period)

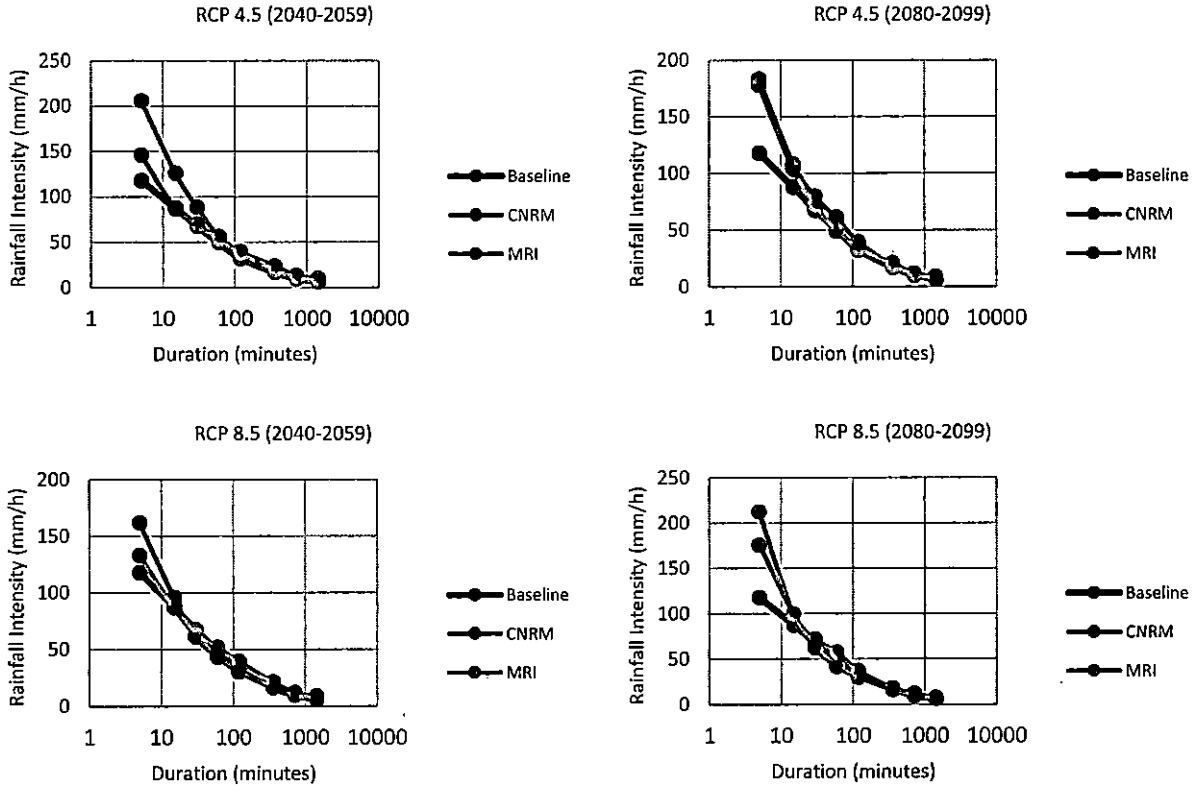

Figure 31 (d) Variability from GCM selection under two RCPs and two time slices (50-yr return period)

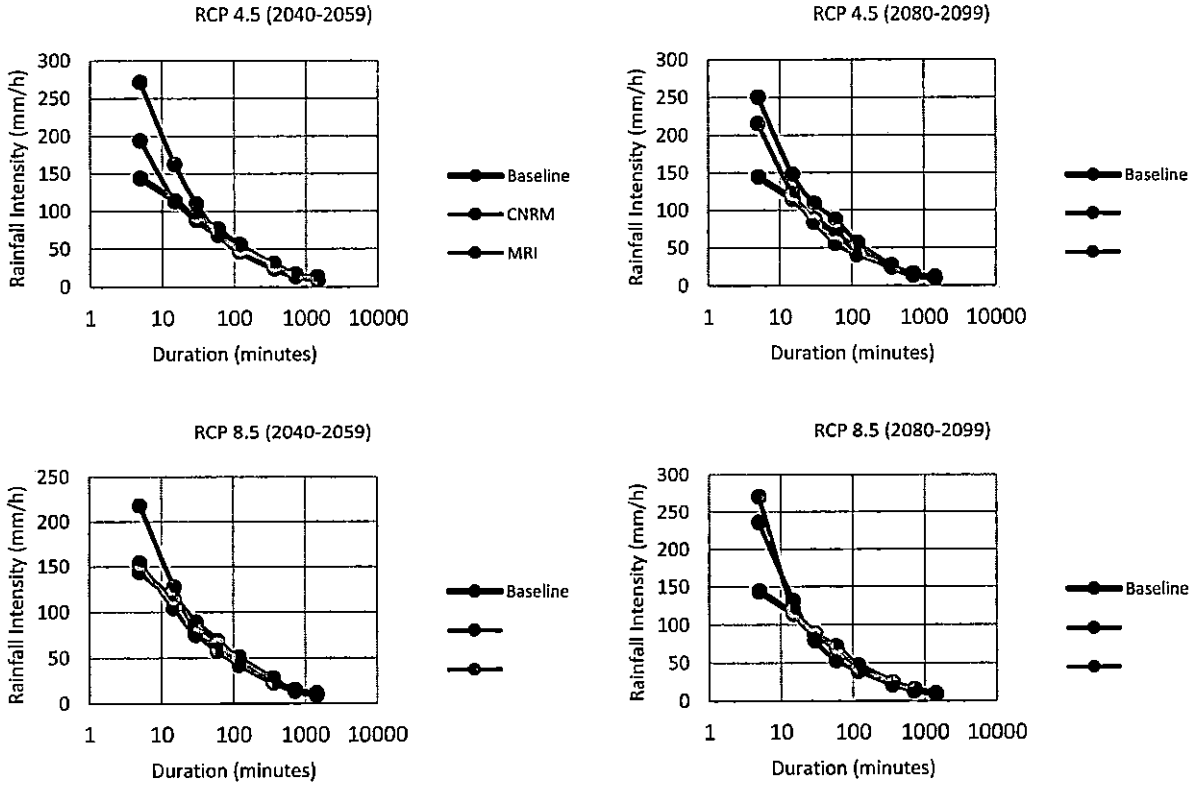

Figure 31 (e) Variability from GCM selection under two RCPs and two time slices (100-yr return period)

When considering the effect of RCPs on the projections towards the century separately, it was observed that the RCP 4.5 being a stabilizing RCP, i.e. its radiative forcing increases and then stabilizes from mid until the end of the 2100 to 4.5 W/m^2, did not exhibit a consistent effect on the sign and magnitude of change of the extreme rainfall intensities. The RCP 8.5 on the other hand has shown a relatively consistent increasing trend for storms 5-min, 15-min, and 30-min which could be related to the nature of this scenario, having a steady radiative forcing increase until the end of 2100 with a magnitude of 8.5 W/m^2. An example of 5-min storm is shown in Figure 32.

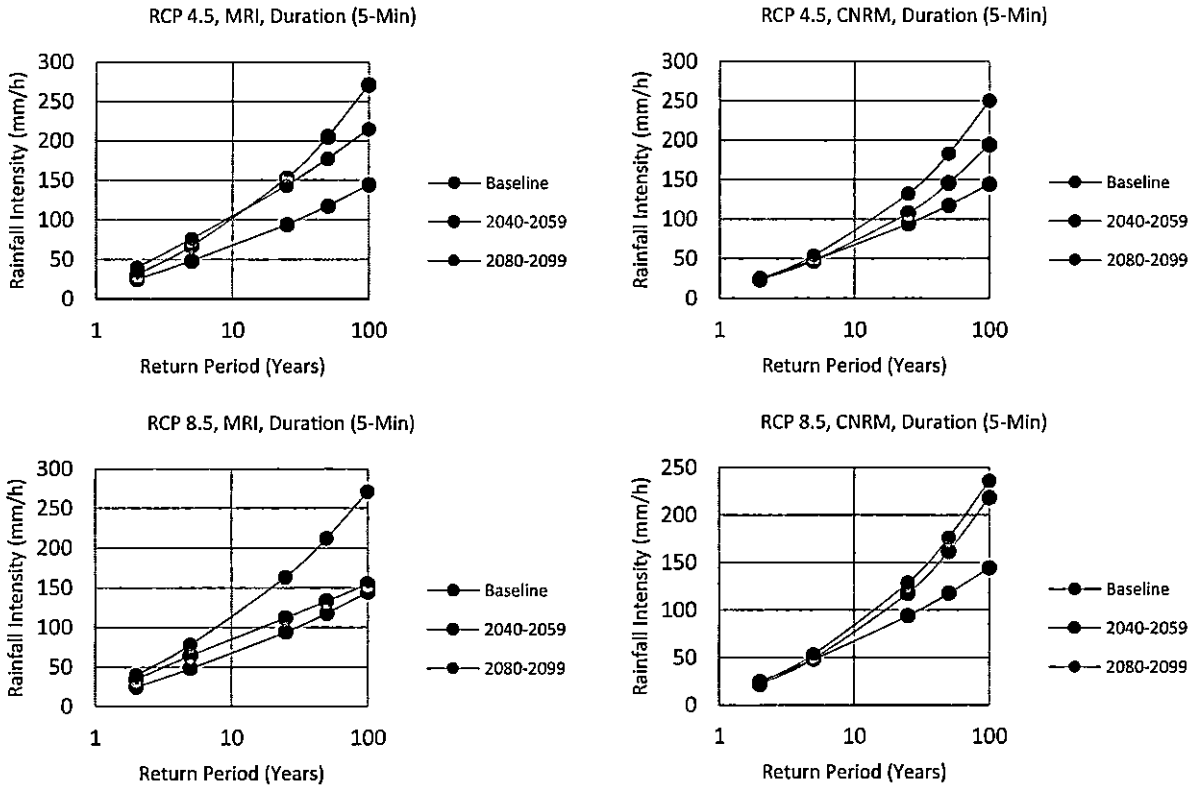

Figure 32 Effect of each RCP on the projections for the two time periods (2040-2059) & (2080-2099)

5.4.2 Variations due to downscaling/disaggregation

The two stage downscaling method is also expected to contribute a level of uncertainty. Unfortunately, the study was limited to the use of one method in producing the IDF curves. Alam and Elshorbagy, (2015) considered Genetic Programming downscaling method based on regression analysis which uses the baseline AMRs of the local scale and relate them with the GCM daily AMRs to generate duration-specific AMR's without generating rainfall time series values. It was found that the results obtained from the combined downscaling-disaggregation and GP methods were in general comparable. Sarr et al (2015) made a comparison study between two downscaling techniques, delta-change method and quantile–quantile transformation for Senegal. The results showed that the effect of the selection of the downscaling technique on storms of return period equal or more than 10 years outweighs the effect that resulted from the selection of the GCM.

5.4.3 Variations due to GEV distribution fitting of the AMR's

Fitting the probability distribution functions on a set of data is a common statistical method in order to understand the behavior of empirical records related to certain phenomenon. The type of the distribution functions and the sample size might cause variations in the results required to be generated. As explained in the future IDF curves section that the sample considered in each scenario for the GEV fitting process comprise the historical AMR's as well. To investigate the probable variation that could be resulted from changing the sample size, each time slice was treated independent of the previous time slices. Appendix B (Table B-2) shows the IDF results for all of the scenarios. For example, by fitting the GEV distribution on the 2080-2099 (i.e. 20 years of AMR's) time slice, the following results (Table 8) were obtained as an average of the two GCM's under the two RCP's:

Table 8 IDF's generated by fitting the GEV distribution to the 20 years sample (2080-2099) independent of previous time slices

	2080-2099				
	2-yr	5-yr	25-yr	50-yr	100-yr
5-min	40	77	169	228	306
15-min	23	42	85	113	149
30-min	16	30	59	76	99
1-hr	11	20	41	54	74
2-hr	7	12	24	32	43
6-hr	4	7	12	15	18
12-hr	2	4	8	10	13
24-hr	1	2	5	6	7

The results show that the lower the sample size the higher the modelled results for the duration 5-min to 1-hr when compared with Table 7. The higher storm durations (2hr-24hr) results were in general lower in the case of smaller size data. These variations in producing the IDF curves due to the fitting of the sample data contribute significantly in the uncertainty associated with this study.

In order to present this variability in a more organized form, the base, maximum and minimum values of averaged IDFs from both approaches are shown in Table 9 as follows.

Table 9 Base, maximum and minimum IDF's from both approaches of GEV fitting

	2-yr			5-yr			25-yr			50-yr			100-yr		
	base	min	max	base	min	max	base	min	max	base	min	max	base	min	max
5-min	25	28	40	48	57	77	94	122	169	118	161	228	144	209	306
15-min	14	17	23	30	35	42	66	75	85	88	99	113	114	127	149
30-min	10	12	16	22	26	30	50	54	59	67	70	76	89	90	99
1-hr	6	8	11	14	17	20	35	38	41	50	51	54	69	67	74
2-hr	4	5	7	8	11	13	22	24	29	32	32	40	46	43	53
6-hr	2	3	4	4	6	7	11	12	16	17	15	22	24	18	29
12-hr	1	2	2	3	4	5	7	8	9	10	10	12	14	13	16
24-hr	1	1	1	2	2	3	4	5	7	7	6	9	10	7	11

CHAPTER 6: CONCLUSIONS AND RECOMMENDATIONS

The Future IDF curves under two GCMs and two RCPs were constructed for Tawi Atair using combined downscaling-disaggregation method. The disaggregation models for the hourly and 5-min time series were developed using the K-nearest neighbor technique. The sampling was performed by considering the window size approach where the optimum window that produced the minimum RMSE value was selected. In the case of Tawi Atair, 57 days and 181 hours were the optimum window sizes for the hourly and 5-min models, respectively.

The two models were then used to disaggregate the future downscaled projections. The downscaling process was conducted by using LarsWG 5.5, a stochastic weather generator which uses the local scale probability distribution to generate synthetic rainfall time series with the same statistical characteristics. The eight scenarios considered in this study was downscaled and disaggregated to 1 hour and 5-min intervals from which the AMRs for different durations (5-min, 15-min, ... , 24-hr) were calculated.

R-extreme was then used to perform fitting the annual maximum rainfalls obtained for all scenarios to GEV distribution function and obtain the shape, scale and location parameters which are necessary to calculate the return levels of each storm return periods considered in this study (2-yr, 5-yr, ... , 100-yr), hence plot the baseline and future IDF curves.

The effect of climate change on the IDF curves was more significant on the shorter durations and high return periods. Moving towards the end of the 21st century, the extreme rainfall intensities were found to be increasing except for the storms with durations higher than 1-hour which could be related to the negative effect of climate change on arid regions where the contribution of high durations storms to the total annual is expected to be decreasing as supported in literature.

The uncertainty level in producing the final results related to different factors were discussed in general. For instance, the contribution of RCP and GCM selection to the uncertainty level was high in general. Different aspects of such variability was discussed. Other factors include the disaggregation downscaling methods and the GEV fitting of the AMRs.

As such and since the reported variations in the future IDF curves are not manageable from engineering point of view for the purpose of engineering design, the average of all scenarios for the two future time slices was presented which would be convenient to somehow address the irregularities associated with the whole process. In that sense, it is recommended to consider more GCMs and more RCPs for broader range of future projections.

It is also recommended to apply different downscaling/disaggregation methods for the sake of verifying the methods performance and quantifying the variations among each other.

Finally, this study has succeeded in employing the combined downscaling-disaggregation method into investigating the climate change-induced variations for the IDF curves in Tawi Atair. The study can still be enhanced considering the recommendations above and expanded to cover more locations in the Sultanate which will provide a reference for the water management systems designers to take the necessary mitigation plans.

References

Abdellatif, M., Atherton, W., Alkhaddar, R. (2013). Application of the stochastic model for temporal precipitation disaggregation for hydrological studies in north western England. Journal of Hydroinformatics, 15, pp. 555-567.

Alexander, L.V., Zhang X., Peterson T.C., Caesar J., Gleason B., Klein Tank A.M.G., Haylock M., Collins D., Trewin B., Rahimzadeh F., Tagipour A., Ambenje P., Rupa Kumar K., Revadekar J. and Griffiths G., (2006). Global observed changes in daily climate extremes of temperature and precipitation. Journal of Geophysical Research, 111 (D05109).

Alam, M.S., Elshorbagy, A. (2015). Quantification of the climate change-induced variations in intensity-duration-frequency curves in the Canadian prairies. Journal of Hydrology, 527, pp. 990–1005.

Al-Habsi M., Gunawardhana L. N., Al-Rawas G., (2014). Trend Analysis of Climate Variability in Salalah. International Journal of Students, 2, pp. 168-171.

Al Mamoon A., Joergensen N.E., Rahman A., Qasem H. (2016). Design rainfall in Qatar: sensitivity to climate change scenarios. Nat. Hazards, 81, pp. 1797–1810.

Al-Rawas, A. G. Valeo, C. (2010). Relationship between wadi drainage characteristics and peak-flood flows in arid northern Oman. Hydrological Sciences Journal, 55, pp. 377–393.

Al-Sarmi, S. H. and Washington, R. (2013). Changes in climate extremes in the Arabian Peninsula: analysis of daily data. International Journal of Climatology, 34, pp. 1329-1345.

Burian, S. J., Durrans, S. R., Tomic, S., Pimmel, R. L., and Wai, C. N. (2000). Rainfall disaggregation using artificial neural networks. Journal of Hydrologic Engineering, ASCE, 5, pp. 299–307.

Busuioc, A., Tomozeiu, R., Cacciamani, C. (2008). Statistical downscaling model based on canonical correlation analysis for winter extreme precipitation events in Emilia-Romagna region. International Journal of Climatology, 28, pp. 449–464.

Chandler, R. E., and Wheater, H. S. (2002). Analysis of precipitation variability using generalized linear models: A case study from the west of Ireland. Water Resources Research, 38, pp. 10-1-10-11.

Danielsson P. E. (1980). Euclidean distance mapping. Computer Graphics and Image Processing, 14, pp. 227–248.

Gunawardhana, L. N., Al-Rawas, A. G., Kazama, S., Al-Najar, K. A. (2015). Assessment of future variability in extreme precipitation and the potential effects on the wadi flow regime. Environmental Monitoring and Assessment, 187, pp. 626-645.

Gunawardhana, L. N., Al-Rawas, A. G., Kwarteng, A. Y., Al-Wardy, M., Charabi, Y. (2017). Potential changes in the number of wet days and its effect on future intense and annual precipitation in northern Oman. Hydrology Research, doi: 10.2166/nh.2017.188.

Hanaish I. (2016). Multivariate Rainfall Disaggregation Using MuDRain Model: Malaysia Experience. International Journal of Civil, Mechanical and Energy Science, 2, pp. 054-067.

Hashmi, M.Z., Shamseldin, A.Y., Melville, B.W. (2009). Downscaling of future rainfall extreme events: a weather generator based approach. In: 18th World IMACS/MODSIM Congress, Cairns, Australia, 13–17 July, 2009.

Hashmi, M.Z., Shamseldin, A.Y., Melville, B.W. (2011). Comparison of SDSM and LARS-WG for Simulation and downscaling of extreme precipitation events in a watershed. Stochastic Environmental Research and Risk Assessment, 25, pp. 475–484.

Hassanzadeh, E., Nazemi, A., Elshorbagy, A. (2014). Quantile-based downscaling of rainfall using genetic programming: application to IDF curves in the City of Saskatoon. Journal of Hydrologic Engineering, 19, pp. 943–955.

Hutchinson, M.F. (1987). Methods of generation of weather sequences. In: Bunting, A.H. (Ed.), Agricultural Environments: Characterization, Classification and Mapping. CAB International, Cambridge.

Jenkinson, A. F. (1955). The frequency distribution of the annual maximum (or minimum) values of meteorological elements. Quarterly Journal of the Royal Meteorological Society, 81, pp. 158–171.

Kwarteng, A. Y., Dorvlo, A. S., Kumar, G.T.V. (2009). Analysis of a 27-year rainfall data (1977-2003) in the Sultanate of Oman. International Journal of Climatology, 29, pp. 605-617.

Lall, U. and Sharma, A. (1996). A nearest neighbour bootstrap for time series resampling. Water Resources Research, 32, pp. 679–693.

Liu, T. (2006). Fast Nonparametric Machine Learning Algorithms for High-dimensional Massive Data and Applications. Doctoral thesis, Carnegie Mellon University, Pittsburgh, PA 15213, USA.

Lu, Y., Qin X. S., Mandapaka P.V., (2015). A Combined weather generator and K-Nearest-Neighbor approach for assessing climate change impact on regional rainfall extremes, International Journal of Climatology, 35, pp. 4493-4508.

Masui T, Matsumoto K, Hijioka Y, Kinoshita T, Nozawa T, Ishiwatari S, Kato E, Shukla PR, Yamagata Y, Kainuma M (2011). An emission pathway to stabilize at 6 W/m^2 of radiative forcing. Climatic Change, 109, pp. 59-76.

Meinshausen M., Smith S. J., Calvin, K., Daniel, J. S., Kainuma, M. L. T., Lamarque, J-F., Matsumoto, K., Montzka, S. A., Raper, S. C. B., Riahi, K., Thomson, A., Velders, G. J. M., van

Vuuren, D. P. P. (2011). The RCP Greenhouse Gas Concentrations and their extension from 1765 to 2300. Climatic Change, 109, pp. 213–241.

Mishra, P. K., Khare, D., Mondal, A., Kundu, S. (2014). Multiple Linear regression based statistical downscaling of daily precipitation in canal command. Climate Change Biodiversity, 1, pp. 73-83. doi: 10.1007/978-4-431-54838-6_6.

Moss, R. H., Edmonds, J. A., Hibbard, K. A., Manning, M. R., Rose, S. K., van Vuuren, D. P., Carter, T. R., Emori, S., Kainuma, M., Kram, T., Meehl, G. A., Mitchell, J. F. B., Nakicenovic, N., Riahi, K., Smith, S. J., Stouffer, R. J., Thomson, A. M., Weyant, J. P., Wilbanks, T. J. (2010). The next generation of scenarios for climate change research and assessment. Nature, 463, pp. 747–756.

Nowak, K., Prairie, J., Rajagopalan, B.,Lall, U. (2010). A nonparametric stochastic approach for multisite disaggregation of annual to daily streamflow. Water Resources Research, 46 (W08529).

Koutsoyiannis, D., Onof, C., Wheater, H. S. (2003). Multivariate rainfall disaggregation at a fine timescale. Water Resources Research, 39, pp. 1-18.

Ormsbee, L. E. (1989). Rainfall disaggregation model for continuous hydrologic modeling. Journal of Hydraulic Engineering, ASCE, 115, pp. 507–525.

Racsko, P., Szeidl, L., Semenov, M. (1991). A serial approach to local stochastic weather models. Ecol Model, 57, pp. 27–41.

Riahi, K., Krey, V., Rao, S., Chirkov, V., Fischer, G., Kolp, P., Kindermann, G., Nakicenovic, N., Rafai, P. (2011). RCP-8.5: Exploring the consequence of high emission trajectories. Climatic Change, 109, pp. 33-57.

Richardson, C. W. (1981). Stochastic Simulation of Daily Precipitation, Temperature and Solar Radiation. Water Resources Research, 17, pp. 182–190.

Rodriguez-Iturbe, I., Cox, D. R., and Isham, V. (1987). Some models for precipitation based on stochastic point processes. Proc. R. Soc. London, Ser. A, 410, pp. 269-288.
Sarr, M. A., Seidoub, O., Tramblayc Y., El Adlounid S., (2015). Comparison of downscaling methods for mean and extreme precipitation in Senegal. Journal of Hydrology: Regional Studies, 4, pp. 369–385.

Sharif, M. and Burn, D. H. (2007). Improved K-nearest neighbor weather generating model. Journal of Hydrologic Engineering, 12, pp. 42-51.

Semenov M. A. and Barrow, E. M. (1997). Use of a stochastic weather generator in the development of climate change scenarios. Climate Change, 35, pp. 397–414.

Semenov, M. A., Brooks, R. J., Barrow, E. M., Richardson, C. W. (1998). Comparison of the WGEN and LARS-WG stochastic weather generators in diverse climates. Climate Research, 10, pp. 95-107.

Semenov, M. A. and Barrow, E. M. (2002). The User Manual of LARS-WG: A Stochastic Weather Generator for Use in Climate Impact Studies, Version 3.0. Rothamsted Research: Hertfordshire, UK.

Semenov, M. A. and Stratonovitch, P. (2010). Use of multi-model ensembles from global climate models for assessment of climate change impacts. Climate Research, 41, pp. 1-14.

Symon, C. (2013). Climate change: actions, trends and implications for business. The IPCC fifth assessment report, pp. 524–582. Cambridge University Press: Working Group 1.

Thomson, A. M., Calvin, K. V., Smith, S. J., Kyle, G. P., Volke, A., Patel P., Delgado-Arias, S., Bond-Lamberty, B., Wise, M. A., Clarke, L. E., Edmonds, J. A. (2011) RCP4.5: a pathway for stabilization of radiative forcing by 2100. Climatic Change, 109, pp. 77-94.

Trenberth, K. E., Dai, A., Rasmussen, R. M., Parsons, D. B. (2003). The changing character of precipitation. Bulletin of the American Meteorological Society, 84, pp. 1205–1217.

Van Vuuren, D. P., Stehfest, E., Den Elzen, M. G. J., Deetman, S., Hof, A., Isaac, M., Goldewijk, K. K., Kram, T., Beltran, A. M., Oostenrijk, R., van Ruijven, B. (2011) RCP2.6: exploring the possibility to keep global mean temperature change below 2°C. Climatic Change, 109, pp. 95–116

Watt, E., Marsalek, J. (2013). Critical review of the evolution of the design storm event concept. Canadian Journal of Civil Engineering, 40, pp. 105–113.

Wheater, H. S., Chandler, R. E., Onof, C. J., Isham, V. S., Bellone, E., Yang, C., Lekkas, D., Lourmas, G., and Segond, M. -L. (2005). Spatial-temporal precipitation modelling for flood risk estimation. Stochastic Environmental Research and Risk Assessment, 19, pp. 403–416.

Wilby, R. L., Dawson, C., Barrow, E. (2002). SDSM — a Decision Support Tool for the Assessment of Regional Climate Change Impacts. Environmental Modelling & Software, 17, pp. 145–157.

Wilby, R. L. and Wigley, T. M. L. (1997). Downscaling general circulation model output: a review of methods and limitations. Progress in Physical Geography, 21, pp. 530–548.

Willems, P. and Vrac, M. (2011). Statistical precipitation downscaling for small-scale hydrological impact investigations of climate change. Journal of Hydrology, 402, pp. 193–205.

WMO, (2009): Guidelines on Analysis of extremes in a changing climate in support of informed decisions for adaptation. WCDMP-No. 72.

Appendix A

```
Sub forloop()
Worksheets("Sheet2").Select
Dim wd As Range
Set wd = Range(Cells(9, 5), Cells(1070, 5))
For k = 1 To 10
Worksheets("Sheet4").Select
Range("AOA6").Select
ActiveCell.Value = Cells(k + 29, 1149).Value
For i = 1 To 30
Worksheets("Sheet2").Select
Range("C1").Value = Cells(1, i + 8).Value
wd = Range("C1").Value
For j = 1 To 1062
Worksheets("Sheet2").Select
Range("E9,E1070").Select
Do While Cells(j + 8, 6).Value < k
If Cells(j + 8, 6).Value < k Then Cells(j + 8, 5).Value = Cells(j + 8, 5).Value + 2
Loop
Next j
Worksheets("Sheet4").Select
Dim pt As PivotTable
For Each pt In ActiveSheet.PivotTables
pt.RefreshTable
Next pt
For Each pt In ActiveSheet.PivotTables
pt.RefreshTable
Next pt
Range("ARF30").Select
Cells(29 + k, 1149 + i).Value = Cells(29, 1146).Value
Next i
Next k
End Sub
```

Figure A-1: Excel Macro Code to automatically record the RMSE value for each window size considered in the K-NN hourly disaggregation model.

Table A-1 RMSE results of all window sizes for the hourly disaggregation model.

window	half window	RMSEs
3	1	0.223526
5	2	0.188481
7	3	0.190011
9	4	0.224396
11	5	0.224057
13	6	0.225251
15	7	0.225251
17	8	0.247221
19	9	0.248726
21	10	0.248155
23	11	0.247996
25	12	0.249014
27	13	0.244742
29	14	0.216194
31	15	0.23044
33	16	0.230455
35	17	0.230974
37	18	0.230974
39	19	0.230974
41	20	0.230974
43	21	0.234719
45	22	0.237644
47	23	0.237644
49	24	0.237644
51	25	0.237644
53	26	0.238278
55	27	0.228972
57	28	0.156023
59	29	0.156023
61	30	0.156023

Table A-2 RMSE results of all window sizes for the Sub-hourly disaggregation model.

window	half window	RMSE:s
3	1	0.186006
5	2	0.184641
7	3	0.321102
9	4	0.319385
11	5	0.14803
13	6	0.14803
15	7	0.14803
17	8	0.148228
19	9	0.148228
21	10	0.148228
23	11	0.148228
25	12	0.148228
27	13	0.148228
29	14	0.148181
31	15	0.148189
33	16	0.148189
35	17	0.148189
37	18	0.148127
39	19	0.138186
41	20	0.139422
43	21	0.139512
45	22	0.139879
47	23	0.138898
49	24	0.139167
51	25	0.125075
53	26	0.125579
55	27	0.125579
57	28	0.126857
59	29	0.126857
61	30	0.126953
63	31	0.126953
65	32	0.126953
67	33	0.126953
69	34	0.126842
71	35	0.126842
73	36	0.126842
75	37	0.126842
77	38	0.115042
79	39	0.115042
81	40	0.115042
83	41	0.115042
85	42	0.115042
87	43	0.115042
89	44	0.115042
91	45	0.115042
93	46	0.115042
95	47	0.115042
97	48	0.115042
99	49	0.065571
101	50	0.065571
103	51	0.065571
105	52	0.065571
107	53	0.065571
109	54	0.065571
111	55	0.065571
113	56	0.065571
115	57	0.064185
117	58	0.064185
119	59	0.064185
121	60	0.064185
123	61	0.064185
125	62	0.064185
127	63	0.064185
129	64	0.064185
131	65	0.064185
133	66	0.064185
135	67	0.064185
137	68	0.064185
139	69	0.064185
141	70	0.064185
143	71	0.064185
145	72	0.064185
147	73	0.064185
149	74	0.064185
151	75	0.064185
153	76	0.064185
155	77	0.064185
157	78	0.064185
159	79	0.064185
161	80	0.064185
163	81	0.064185
165	82	0.064185
167	83	0.064185
169	84	0.065361
171	85	0.065361
173	86	0.06394
175	87	0.06394
177	88	0.06394
179	89	0.06394
181	90	0.06394
183	91	0.066533
185	92	0.066533
187	93	0.066533
189	94	0.071492
191	95	0.071492
193	96	0.071492
195	97	0.071492
197	98	0.071492
199	99	0.071492
201	100	0.071492
203	101	0.071492
205	102	0.071492
207	103	0.071492
209	104	0.071492
211	105	0.071492
213	106	0.071492
215	107	0.071492
217	108	0.071492
219	109	0.071492
221	110	0.071492
223	111	0.072128
225	112	0.072128
227	113	0.072128
229	114	0.072128
231	115	0.072128
233	116	0.072128
235	117	0.072128
237	118	0.072128
239	119	0.072128
241	120	0.072128

Appendix B

Table B-1 IDF's obtained by considering AMR's of each scenario plus the previous AMR's.

			2040-2059						2080-2099				
RCP	GCM		2-yr	5-yr	25-yr	50-yr	100-yr		2-yr	5-yr	25-yr	50-yr	100-yr
RCP 4.5	CNRM	5-min	24	48	108	146	194		25	54	132	183	250
		15-min	14	29	65	86	113		14	31	78	108	148
		30-min	10	21	51	70	95		10	23	57	80	109
		1-hr	6	14	37	54	77		6	15	42	61	87
		2-hr	4	9	26	38	56		4	10	27	39	57
		6-hr	2	5	14	20	29		2	5	13	19	27
		12-hr	1	3	8	12	16		1	3	8	11	16
		24-hr	1	2	5	8	11		1	2	5	7	10
	MRI	5-min	31	67	153	205	271		40	76	144	178	215
		15-min	20	43	95	126	163		25	47	85	103	123
		30-min	15	33	69	88	110		19	35	61	72	84
		1-hr	10	21	44	56	70		13	24	41	48	56
		2-hr	6	14	30	39	50		8	15	28	34	41
		6-hr	4	8	18	24	31		5	9	17	21	25
		12-hr	2	5	10	13	16		3	5	10	11	13
		24-hr	1	3	7	10	13		2	3	7	9	11
RCP 8.5	CNRM	5-min	22	49	117	161	218		23	53	129	176	236
		15-min	13	30	71	96	127		14	32	74	99	131
		30-min	9	21	46	61	79		10	22	48	62	79
		1-hr	6	13	32	43	58		7	15	32	41	53
		2-hr	4	8	21	30	42		4	9	22	30	39
		6-hr	2	4	11	16	23		2	5	12	16	21
		12-hr	1	3	7	11	15		1	3	8	12	16
		24-hr	1	2	4	6	9		1	2	5	7	9
	MRI	5-min	35	64	112	133	154		40	78	163	212	271
		15-min	20	38	70	86	104		24	44	81	99	119
		30-min	14	28	52	63	75		17	32	59	72	86
		1-hr	10	20	41	52	64		11	22	45	57	72
		2-hr	6	14	30	39	51		7	14	28	37	47
		6-hr	3	7	16	21	27		4	7	14	18	22
		12-hr	2	5	9	12	14		2	4	8	10	13
		24-hr	1	3	6	9	11		1	2	5	7	10

Table B-2 IDF's obtained by considering AMR's of each scenario independent of the previous AMR's.

			2040-2059						2080-2099				
RCP	GCM		2-yr	5-yr	25-yr	50-yr	100-yr		2-yr	5-yr	25-yr	50-yr	100-yr
RCP 4.5	CNRM	5-min	23	47	118	169	240		27	66	173	245	339
		15-min	14	28	66	91	125		13	35	99	143	205
		30-min	9	19	51	75	108		9	25	68	98	139
		1-hr	6	14	39	60	89		6	16	49	75	111
		2-hr	4	9	28	44	67		3	9	28	43	64
		6-hr	2	5	15	23	35		2	5	13	17	23
		12-hr	2	3	9	14	20		1	3	8	11	16
		24-hr	1	2	6	9	12		1	2	4	6	8
	MRI	5-min	39	85	194	259	340		55	84	118	129	138
		15-min	26	56	115	146	182		34	48	62	66	69
		30-min	21	42	80	97	116		25	35	44	46	48
		1-hr	13	27	48	58	67		18	27	34	36	37
		2-hr	9	18	34	41	49		10	16	22	24	26
		6-hr	5	11	21	25	30		6	10	14	16	17
		12-hr	3	7	11	13	15		4	6	8	9	10
		24-hr	2	5	9	11	13		2	3	6	7	8
RCP 8.5	CNRM	5-min	19	47	134	196	283		25	62	154	212	285
		15-min	12	29	76	107	149		14	34	83	114	154
		30-min	8	19	45	60	79		10	24	52	69	88
		1-hr	6	13	30	40	53		8	17	32	39	47
		2-hr	3	7	21	30	43		6	12	23	28	33
		6-hr	2	4	11	16	23		3	6	13	16	19
		12-hr	1	3	7	11	17		2	5	10	13	16
		24-hr	1	1	4	6	9		1	2	5	7	9
	MRI	5-min	44	77	121	137	153		52	96	229	326	462
		15-min	24	43	74	88	102		31	49	97	129	169
		30-min	17	32	53	62	70		21	34	69	92	122
		1-hr	13	24	44	54	65		13	21	47	68	99
		2-hr	9	17	34	43	53		7	11	24	34	50
		6-hr	5	9	18	23	28		4	6	10	12	14
		12-hr	3	6	10	12	13		2	3	6	7	8
		24-hr	2	4	7	9	11		1	2	3	4	4